EAVN Status Report for the 2024A Semester

EAVN User Support Team, KASI, NAOJ, NGII, SHAO, XAO, YNAO, NGII, NARIT, Ibaraki University, and Yamaguchi University

September 19, 2023

Major revisions since the 2023B semester

- Nanshan 26-m telescope will be available at C-band from the 2024A semester on a shared-risk basis (Sections 2.2.9 and 2.3.9).
- The 1-beam hybrid mode is restarted in the 2024A semester (Sections 3.6 and 4.3).
- Nobeyama 45-m and Kunming 40-m telescopes will not join the EAVN observations in the 2024A semester (Sections 2.2.3, 2.2.10, 3.1, and 3).

Contents

1	Intr	on	5	
2	Sys	tem		5
	2.1	Array		5
	2.2	Anteni	nas	10
		2.2.1	Brief Summary of VERA Antennas	10
		2.2.2	Brief Summary of KVN Antennas	10
		2.2.3	Nobeyama 45-m Telescope	10
		2.2.4	Takahagi 32-m Telescope	11
		2.2.5	Hitachi 32-m Telescope	11
		2.2.6	Yamaguchi 32-m Telescope	11
		2.2.7	Tianma 65-m Telescope	11
		2.2.8	Sheshan 25-m Telescope	12
		2.2.9	Nanshan 26-m Telescope	12
		2.2.10	Kunming 40-m Telescope	12
		2.2.11	Sejong 22-m Telescope	13
		2.2.12	Aperture Efficiency	15
		2.2.13	Beam Pattern and Size	16
	2.3	rers	19	
		2.3.1	Brief Summary of VERA Receiving System	19
		2.3.2	Brief Summary of KVN Receiving System	21
		2.3.3	Brief Summary of NRO45 Receiving System	21
		2.3.4	Brief Summary of TAK32 Receiving System	22
		2.3.5	Brief Summary of HIT32 Receiving System	23
		2.3.6	Brief Summary of YAM32 Receiving System	24
		2.3.7	Brief Summary of TMRT65 Receiving System	24
		2.3.8	Brief Summary of SHRT25 Receiving System	25
		2.3.9	Brief Summary of NSRT26 Receiving System	25
		2.3.10	Brief Summary of KMRT40 Receiving System	25
		2.3.11	Brief Summary of KSJ Receiving System	26
	2.4		l Signal Processing	28
	2.5	Record	ders	28
		2.5.1	Note on the Data Storage Capacity	29
	2.6	Correla		29
		2.6.1	Note for the C2 Mode	29
	2.7	Calibra		33
		2.7.1	Delay and Bandpass Calibration	33

		2.7.2	Gain Calibration	33						
		2.7.3	Polarization Calibration	35						
		2.7.4	Pointing Correction	35						
	2.8	Geode	tic Measurement	35						
		2.8.1	Brief Summary of VERA Geodetic Measurement	35						
		2.8.2	Brief Summary of KVN Geodetic Measurement	36						
3	Obs	erving	Proposal	37						
	3.1	Call fo	or Proposals (CfP)	37						
		3.1.1	Total telescope time and maximum of total request time	37						
		3.1.2	Term of EAVN observation	39						
		3.1.3	Possible array configuration	39						
	3.2	Propos	sal Submission	39						
	3.3	Special Condition for Selecting Proposals								
	3.4	Policy	of Recovery Observations	40						
	3.5	Policy	of One-year-long Proposals	41						
	3.6	Observation Mode								
	3.7	Target	of Opportunity (ToO) Observations	41						
	ar Resolution and Largest Detectable Angular Scale	42								
	3.9	Sensiti	ivity	43						
	3.10	Calibr	ator Information	47						
	3.11	Data A	Archive	49						
4	Not	es for	Special Modes	51						
	4.1	Dual (Circular Polarization	51						
	4.2	Phase-	referencing and Astrometry	51						
		4.2.1	Fast Switching	51						
		4.2.2	Notification for Switching Cycle in C-band	51						
		4.2.3	Separation Angle between Target and Phase Reference	52						
		4.2.4	Tropospheric Calibration with GPS or JMA or Geodetic Blocks	52						
		4.2.5	Astrometric Accuracy	53						
		4.2.6	Baseline Length	57						
		4.2.7	An accurate delay model for astrometry	57						
		4.2.8	Data Reduction	57						
	4.3	1-bear	n Hybrid (K/Q/W) Mode	57						
	4.4	Wide-	field Imaging Mode	58						
	4.5	Simult	caneous K/Q Band Mode	59						
	4.6	Condi	tion on the Usage of Nobeyama 45-m Telescope	50						

5	Obs	Observation and Data Reduction								
	5.1	Preparation of an EAVN Observation								
		5.1.1 Sample Key Files for NRAO sched	62							
	5.2	Observation and Correlation	62							
	5.3	Data Reduction								
		5.3.1 Sample AIPS Recipes								
	5.4	Policy of User Support	63							
	5.5	Acknowledgment	63							
	5.6	Further Information	64							

1 Introduction

This document describes the current observational capabilities as of 2024 September, and available observing time of the East Asian VLBI Network (EAVN). EAVN is an international collaborative VLBI array operated by Korea Astronomy and Space Science Institute (KASI), National Astronomical Observatory of Japan (NAOJ), Shanghai Astronomical Observatory (SHAO; China), Xinjiang Astronomical Observatory (XAO; China), Yunnan Observatories (YNAO; China), and National Geographic Information Institute (NGII; Korea), and the National Astronomical Research Institute of Thailand (Public Organization; Thailand).

EAVN invites proposals for open-use observations to be carried out from January 16, 2024 to June 15, 2024 (2024A semester). From the 2024A semester, C-band observations with the Nanshan 26-m telescope will be newly open for common-use programs on a shared-risk basis. The total observing time of 500 hours is provided for EAVN open-use operation to proposers, while the available machine time of each telescope is different between each other. Please refer to Table 9 in Section 3 for more details.

In the 2024A semester, EAVN is operated using 14 telescopes, all four 20-m telescopes of VERA, Takahagi 32-m, Hitachi 32-m, and Yamaguchi 32-m telescopes in Japan, all three 21-m telescopes of KVN and Sejong 22-m in Korea, Tianma 65-m, Sheshan 25-m, and Nanshan 26-m in China. Two telescopes, Nobeyama 45-m and Kunming 40-m telescopes, do not join the EAVN observations in the 2024A semester due to the instrumental problems (Sections 2.2.3 and 2.2.10). Figure 1 shows location of EAVN telescopes which participate in open-use observations of EAVN in the 2024A semester.

This status report summarizes general information about EAVN and the performance of each telescope/array, and how to prepare and submit proposals for EAVN. Please refer to the latest report for the overall performance of EAVN [4].

2 System

2.1 Array

In the 2024A semester, 14 radio telescopes (KVN 3 × 21 m, VERA 4 × 20 m, Takahagi 32 m, Hitachi 32 m, Yamaguchi 32 m, Tianma 65 m, Sheshan 25 m, Nanshan 26 m, and Sejong 22 m) are available for EAVN open use, as shown in Figure 1. Nobeyama 45 m, and Kunming 40 m telescopes will not be available in the 2024A semester due to the instrumental problems (Sections 2.2.3 and 2.2.10). Three observing frequencies, 6.7 (C-band), 22 (K-band) and 43 GHz (Q-band), are opened in the 2024A semester. Dual-polarization observations at K-band and Q-band will be open for up to 8 EAVN antennas in the shared-risk mode. Details of the polarization observations will be described in this Status Report (subsections in Sections 2, 3, and 4.1).

KaVA (KVN and VERA Array) is a core array of EAVN, which consists of 7 antenna sites in VERA-Mizusawa, VERA-Iriki, VERA-Ogasawara, VERA-Ishigakijima, KVN-Yonsei, KVN-Ulsan and KVN-Tamna with 21 baselines in 2024A. Dual-polarization observations at K-band and Q-band are open for all the KaVA 7 antennas. The maximum



Figure 1: Location of EAVN sites for the 2024A semester, including the Korea-Japan Correlation Center at KASI (Korea) and Mizusawa VLBI observatory (NAOJ, Japan), overlaid on 'the Blue Marble' image (credit of the ground image: NASA's Earth Observatory).

baseline length of KaVA is 2270 km between VERA-Mizusawa and VERA-Ishigakijima stations, and the minimum baseline length is 305 km between KVN-Yonsei and KVN-Ulsan stations. The maximum angular resolution expected from the baseline length of KaVA is 6.0 mas for C-band (VERA-Ogasawara – KVN-Ulsan baseline), 1.2 mas for K-band and about 0.6 mas for Q-band. The maximum angular resolution is improved to be 1.8 mas at C-band and 0.55 mas at K-band for EAVN (the longest baseline of 5100 km for VERA-Ogasawara – Nanshan baseline for both bands), and that at Q-band was identical to that of VERA (0.63 mas for VERA-Mizusawa – VERA-Ishigakijima baseline) for the full-array of EAVN. Sejong 22-m telescope newly participates in the open-use program from the 2022A semester, resulting in making the minimum baseline length in EAVN of 120 km between Sejong and KVN-Yonsei stations. The geographic locations and coordinates of EAVN antennas in the coordinate system of epoch 2009.0 are summarized in Table 1. Figures 2 and 3 show examples of uv plane coverage for KaVA and EAVN, respectively. Figure 4 shows the elevation angle of each EAVN antenna as a function of hour angle.

The coordinates and averaged velocities of KaVA sites in Table 2 are predicted values at the epoch of January 1, 2018. Reference frame of these coordinates is ITRF2014. The rates of the coordinates of Mizusawa, Iriki, Ogasawara and Ishigakijima are the average value of change of the coordinates from April 16, 2016 to May 26, 2018, after

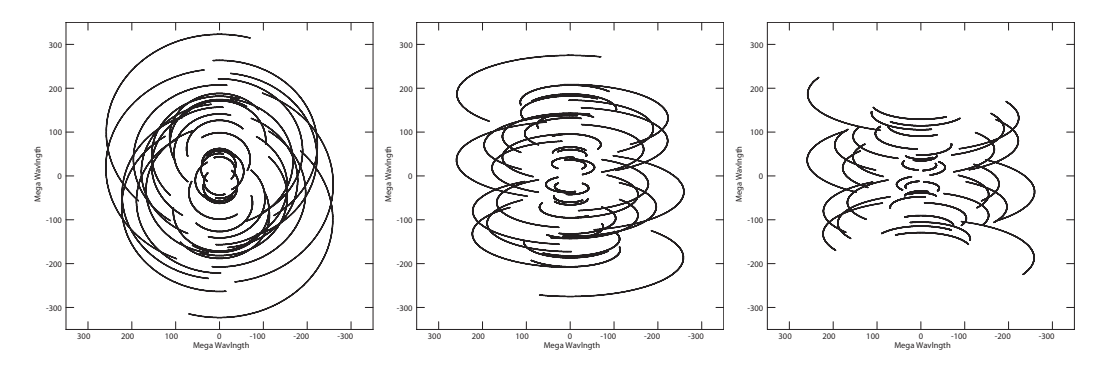


Figure 2: Examples of (u, v) coverage for a KaVA observation at Q-band with the source's declination of $+60^{\circ}$ (left panel), $+20^{\circ}$ (center panel), and -20° (right panel). Total observation duration of 10 hours and the antenna's lower elevation limit of 15° are assumed for all cases.

the 2016 Kumamoto Earthquake $(M_j = 7.3)$. The 2011 off the Pacific coast of Tohoku Earthquake $(M_j = 9.0)$ brought the co-seismic large step and non-linear post-seismic movement to the coordinates of Mizusawa. Co-seismic steps of the coordinates of Mizusawa are dX = -2.0297 m, dY = -1.4111 m and dZ = -1.0758 m. The creeping continues still now, though decreased. The changes of coordinates by the post-seismic creeping are dX = -1.2148 m, dY = -0.6402 m and dZ = -0.3042 m in total from March 12, 2011 to January 1, 2020.

Table 1: Geographic locations of each EAVN antenna.

	East	North	Ellipsoidal			
Site	Longitude	Latitude	Height	X	Y	${ m Z}$
	[° ′ ″]	[° ′ ′′]	[m]	[m]	[m]	[m]
Nobeyama ^a	138 28 21.2	35 56 40.9	1350	-3871025.4987	3428107.3984	3724038.7361
$\operatorname{Takahagi}^b$	$140\ 41\ 41.0$	$36\ 41\ 54.5$	117.1	-3961882.0160	3243372.5190	3790687.4570
$\mathrm{Hitachi}^b$	$140\ 41\ 31.6$	$36\ 41\ 50.8$	120.2	-3961789.1650	3243597.5310	3790597.7000
Yamaguchi	$131\ 33\ 25.5$	$34\ 12\ 57.7$	133	-3502544.587	3950966.235	3566381.192
$Tianma^c$	$121\ 08\ 09.4$	$31\ 05\ 31.6$	49.2	-2826708.6380	4679237.0440	3274667.5330
Sheshan	$121\ 11\ 58.8$	$31\ 05\ 57.0$	29.4	-2831687.4306	4675733.4626	3275327.4941
Nanshan	$87\ 10\ 40.4$	$43\ 28\ 15.6$	2029.4	228310.1700	4631922.7550	4367064.0740
Kunming^c	$102\ 47\ 45.6$	$25\ 01\ 40.8$	1974.0	-1281152.8860	5640864.4013	2682653.4578
$Mizusawa^d$	$141\ 07\ 57.3$	$39\ 08\ 00.7$	116.6	-3857244.9731	3108782.9179	4003899.1695
Iriki^d	$130\ 26\ 23.6$	$31\ 44\ 52.4$	573.6	-3521719.8813	4132174.6817	3336994.1132
$Ogasawara^d$	$142\ 12\ 59.8$	$27\ 05\ 30.5$	273.1	-4491068.3826	3481545.2394	2887399.8018
Ishigakijima d	$124\ 10\ 15.6$	$24\ 24\ 43.8$	65.1	-3263995.2619	4808056.3902	2619948.6347
Y onsei d	$126\ 56\ 27.4$	$37\ 33\ 54.9$	139	-3042281.0183	4045902.6730	3867374.3296
$Ulsan^d$	$129\ 14\ 59.3$	$35\ 32\ 44.2$	170	-3287268.6453	4023450.1367	3687379.9886
Tamna^d	$126\ 27\ 34.4$	$33\ 17\ 20.9$	452	-3171731.6665	4292678.5393	3481038.7880
Sejong^e	$127\ 18\ 11.0$	$36\ 31\ 22.0$	156	-3110079.9600	4082066.7340	3775076.8320

^aThe position was measured in late 2016.

The antenna positions of KVN are regularly monitored by geodetic VLBI observations in collaboration with VERA.

 $[^]b$ The position was measured in March 2020.

^cThe epoch of the coordinate is January 1, 2014.

 $^{^{}d}$ The epoch of the coordinates is January 1, 2019.

 $[^]e\mathrm{The}$ position was measured in October 2014.

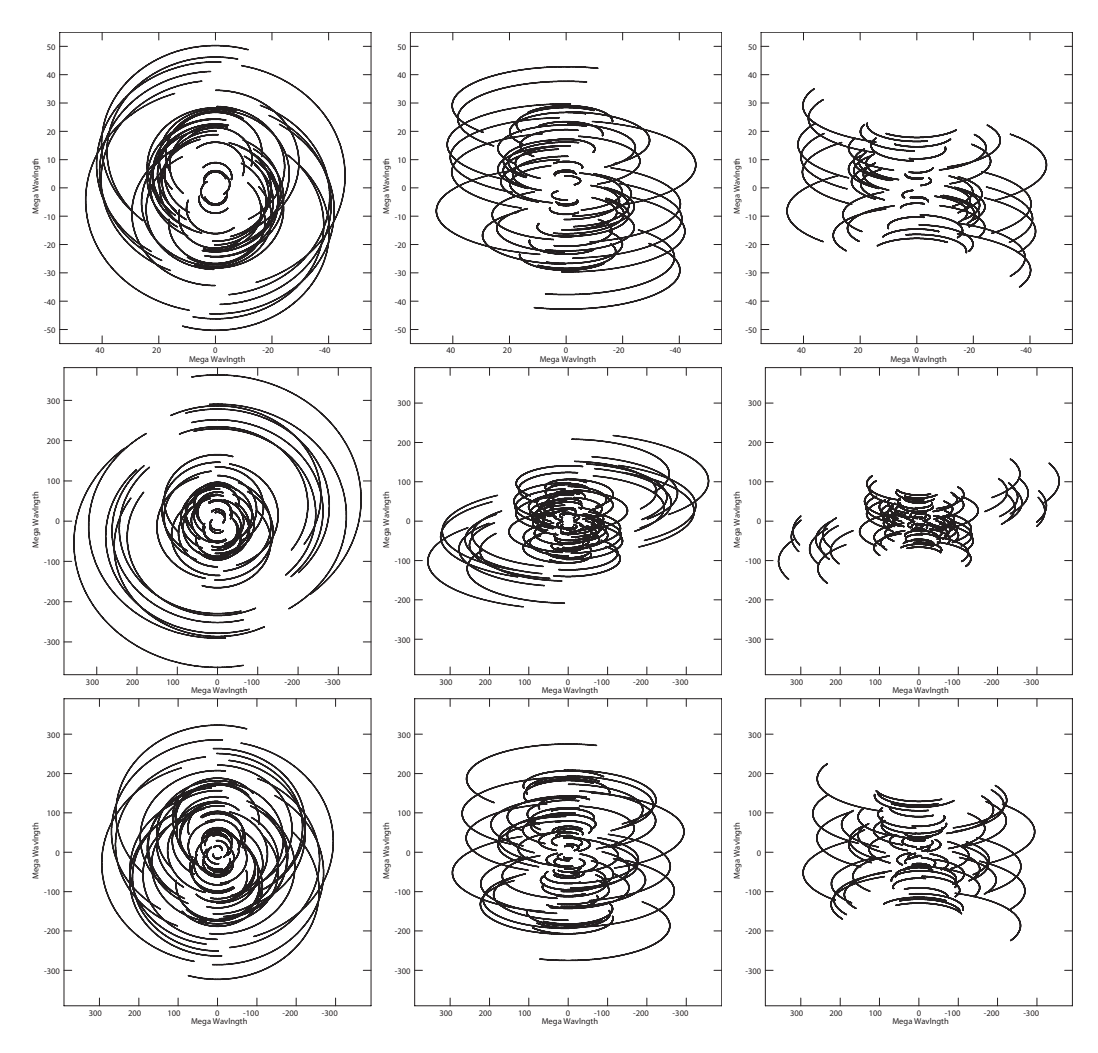


Figure 3: Examples of (u, v) coverage for an EAVN observation with full array configuration in the 2024A semester at C-band (upper panels), K-band (middle panels) and Q-band (lower panels) with the source's declination of $+60^{\circ}$ (left panels), $+20^{\circ}$ (center panels), and -20° (right panels). Total observation duration of 10 hours and the antenna's lower elevation limit of 15° are assumed for all cases.

Table 2: Station code and average velocity of each KaVA antenna.

Site	$IVS2^a$	$IVS8^b$	CDP^c	$\Delta X [m/yr]^d$	$\Delta Y [m/yr]^d$	$\Delta Z [m/yr]^d$
Mizusawa	Vm	VERAMZSW	7362	-0.0433	-0.0138	-0.0047
Iriki	Vr	VERAIRIK	7364	-0.0159	-0.0049	-0.0098
Ogasawara	Vo	VERAOGSW	7363	0.0363	0.0242	0.0119
Ishigakijima	$V_{\rm S}$	VERAISGK	7365	-0.0303	-0.0003	-0.0486
Yonsei	Ky	KVNYONSE		-0.0121	-0.0042	-0.0052
Ulsan	Ku	KVNULSAN		-0.0117	-0.0072	-0.0028
Tamna	Kt	KVNTAMNA		-0.0169	-0.0012	-0.0024

^aIVS 2-characters code

^bIVS 8-characters code

^cCDP (NASA Crustal Dynamics Project) code

^dThe epoch of the coordinates is January 01, 2018. Average speed was obtained from the VLBI data from January 01, 2018 to January 1, 2019.

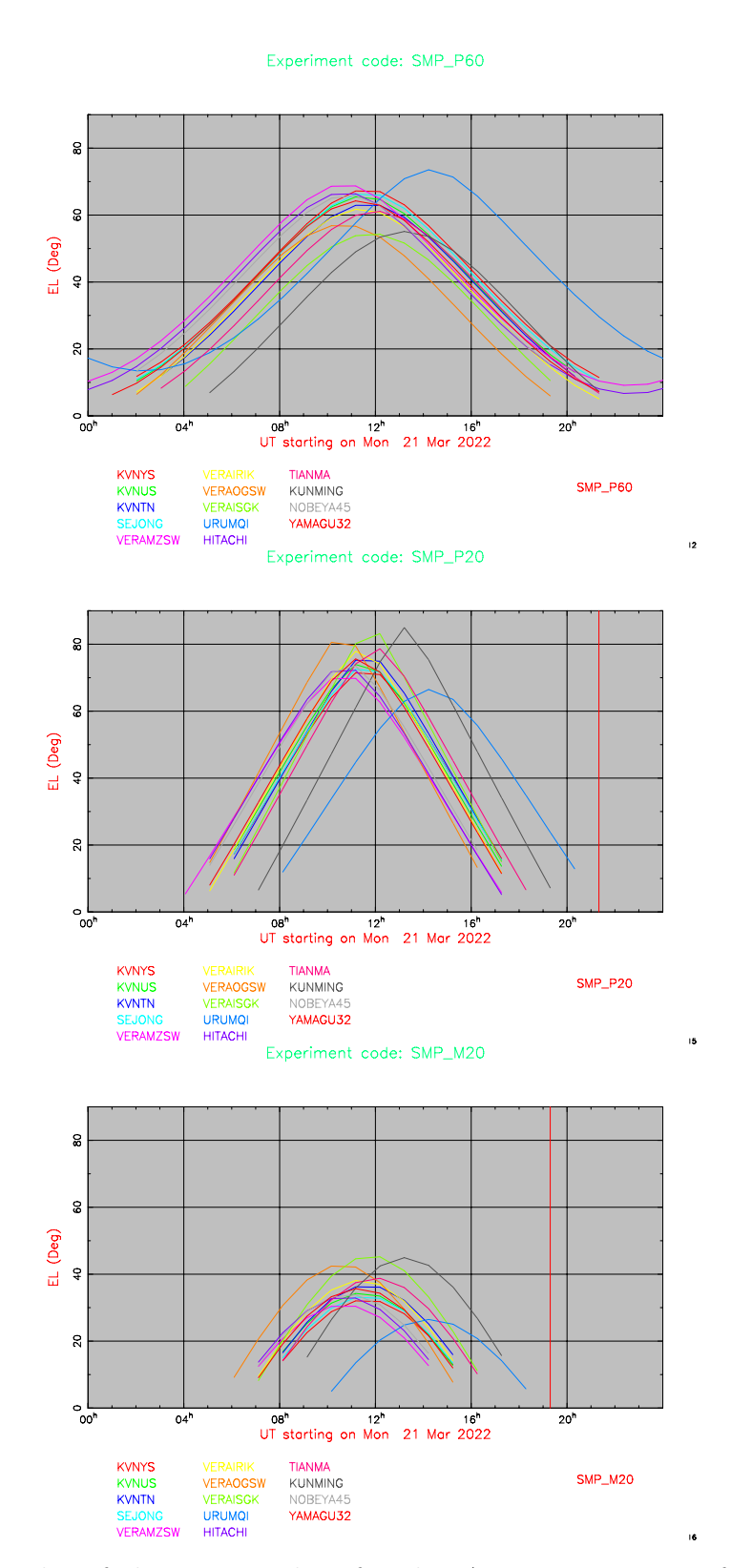


Figure 4: Examples of elevation angles of each EAVN antenna as a function of hour angle for the source's declination of $+60^{\circ}$ (top panel), $+20^{\circ}$ (middle panel), and -20° (bottom panel). Note that the elevation angle plot for Sheshan and Takahagi is almost identical to that for Tianma and Hitachi, respectively, because of their positional proximity.

2.2 Antennas

2.2.1 Brief Summary of VERA Antennas

All the telescopes of VERA have the same design, being a Cassegrain-type antenna on AZ-EL mount. Each telescope has a 20 m diameter dish with a focal length of 6 m, and with a sub-reflector of 2.6 m diameter. The dual-beam receiver systems are installed at the Cassegrain focus. Two receivers are set up on the Stewart-mount platforms, which are sustained by steerable six arms, and with such systems one can simultaneously observe two adjacent objects with a separation angle between 0.32 and 2.2 deg. The whole receiver systems are set up on the field rotator (FR), and the FR rotate to track the apparent motion of objects due to the earth rotation. Table 3 summarizes the ranges of elevation (EL), azimuth (AZ) and field rotator angle (FR) with their driving speeds and accelerations. In the case of single beam observing mode, one of two beams is placed at the antenna vertex (separation offset of 0 deg).

2.2.2 Brief Summary of KVN Antennas

The KVN antennas are also designed to be a shaped-Cassegrain-type antenna with an AZ-EL mount. The telescope has a 21 m diameter main reflector with a focal length of 6.78 m. The main reflector consists of 200 aluminum panels with a manufacturing surface accuracy of about 65 μ m. The slewing speed of the main reflector is 3 °/sec, which enables fast position-switching observations (Table 3). The sub-reflector position, tilt, and tip are remotely controlled and modeled to compensate for the gravitational deformation of the main reflector and for the sagging-down of the sub-reflector itself.

2.2.3 Nobeyama 45-m Telescope

While the Nobeyama 45 m telescope will not be available in the 2024A semester due to the problem in the hydrogen maser operated by the Mizusawa VLBI Observatory of NAOJ, detailed information is summarized in this section for references.

The Nobeyama 45-m Telescope (hereafter NRO45) is one of the largest millimeter radio telescopes in the world. It has a Cassegrain-Coudé optics. The paraboloidal main reflector consists of about 600 pieces of panels, each of which has a surface accuracy of about 60 microns, and the deviation of the whole antenna from an ideal paraboloid is about 90 microns. The sub-reflector has a diameter of 4 m with a convex hyperboloid surface, the position of which is computer-controlled to follow the moving focal point because the main reflector deforms as the elevation angle changes. The slewing speed of the telescope is $\sim 20^{\circ}/\text{min}$ (i.e., $0.3^{\circ}/\text{sec}$). The (EL, AZ) driving ranges are also summarized in Table 3. According to the status report of NRO45, observers are required to conduct a pointing measurement and correction every 1 - 1.5 hours. In addition, it is appropriate to conduct a pointing measurement and correction every 30 minutes during the sunrise and sunset when the outside temperature changes drastically. The pointing accuracy above is achievable for wind speed of less than 4 m/s. It can be degraded if a wind velocity exceeds 10 m/s. Users are recommended to avoid observing targets located within 30 degrees from the Sun because the thermal deformation of the antenna degrades the pointing accuracy. Users who would like to observe the Sun or targets near the Sun should take care of them. More details on the NRO45 can be found in the Nobeyama Radio Observatory official website [2].

2.2.4 Takahagi 32-m Telescope

The Takahagi 32-m Telescope (hereafter TAK32) has a shaped Cassegrain-Coude-type design with a 32-m diameter main reflector and a 2.9-m sub-reflector on Az-El mount. The telescope was constructed in 1992. Cryogenically-cooled receivers at 2 frequency bands (6 – 9 GHz and 21 – 25 GHz) are equipped. The surface accuracy of the main reflector is < 0.64 mm rms at the antenna elevation angle of 35 deg, and 1.6 mm at other antenna elevation angles. The surface accuracy of the sub-reflector is < 0.2 mm rms. The slewing rates of the main reflector is 0.07 deg/sec, as shown in Table 3. The tentative value of aperture efficiency of TAK32 is 30% at K-band (see Table 4; [21]). Although TAK32 can point to the El range of $5^{\circ} \leq El \leq 88^{\circ}$, we recommend to use at the El range of $15^{\circ} \leq El \leq 85^{\circ}$ because the pointing accuracy is not secured at $El \leq 15^{\circ}$.

2.2.5 Hitachi 32-m Telescope

The Hitachi 32-m Telescope (hereafter HIT32) has a shaped Cassegrain-Coude-type design with a 32-m diameter main reflector and a 2.9-m sub-reflector on Az-El mount. The telescope was constructed in 1983. Cryogenically-cooled receivers at 2 frequency bands (6 – 9 GHz and 21 – 25 GHz) are equipped. The surface accuracy of the main reflector is < 0.64 mm rms at the antenna elevation angle of 35 deg, and 1.6 mm at other antenna elevation angles. The surface accuracy of the sub-reflector is < 0.2 mm rms. The slewing rates of the main reflector is 0.2 deg/sec, as shown in Table 3. The value of aperture efficiency of HIT32 is 60-75% at C-band (see Table 4; [21]). Although HIT32 can point to the El range of $5^{\circ} \leq El \leq 88^{\circ}$, we recommend to use at the El range of $15^{\circ} \leq El \leq 85^{\circ}$ because the pointing accuracy is not secured at $El \leq 15^{\circ}$.

2.2.6 Yamaguchi 32-m Telescope

The Yamaguchi 32-m Telescope (hereafter YAM32) has a shaped Cassegrain-Coude-type design with a 32-m diameter main reflector and a 2.9-m sub-reflector on Az-El mount. The telescope was constructed in 1979. A cryogenically-cooled receiver for 6 and 8 GHz observation is equipped. The surface accuracy of the main reflector is < 0.64 mm rms at the antenna elevation angle of 35 deg, and 1.6 mm at other antenna elevation angles. The surface accuracy of the sub-reflector is < 0.2 mm rms. The slewing rates of the main reflector is 0.25 deg/sec, as shown in Table 3. The value of aperture efficiency of YAM32 is 60-70% at C-band (see Table 4).

2.2.7 Tianma 65-m Telescope

The Tianma 65-m Telescope (hereafter TMRT65) has a shaped Cassegrain-type design with a 65-m diameter main reflector and a 6.5-m sub-reflector on Az-El mount. The main reflector consists of 1008 aluminum panels deploying an active surface control system with 1104 actuators. The prime mirror achieves a surface accuracy of about 0.3 mm rms after compensating the gravitational deformation in real time by the active

surface control system. The secondary mirror has a surface error of 0.1 mm rms. A rotatable receiver cabin with the feeds covering frequency range from S-band (2 GHz) to Q-band is mounted at the Cassegrain focus, while the L-band (1.6 GHz) feed is off focus mount separately. The slewing rates of the main reflector are 0.5° /sec in azimuth and 0.3° /sec in elevation, as shown in Table 3. An overhead time of 10 seconds is recommended to settle the antenna on source.

Dual-beam receivers are installed in TMRT65 at both K- and Q-bands. These two beams have a fixed separation angle of 140 arcsec at K-band and 100 arcsec at Q-band. One of the beams is placed at the antenna focus for VLBI observations. The measured beam sizes (HPBW) are listed in Table 4.

2.2.8 Sheshan 25-m Telescope

The Sheshan 25-m Telescope (hereafter SHRT25) is a Cassegrain-type beam wave-guide antenna. The telescope has been in operation since 1987 and is located ~ 6.1 kilometers from TMRT65. Current receiver system include a room-temperature C-band (6.7 GHz) receiver and a cooled S/X co-axis feed receiver. The main surface accuracy is 0.65 mm rms. The slewing speed are $1.0^{\circ}/\text{sec}$ in azimuth and $0.6^{\circ}/\text{sec}$ in elevation, as shown in Table 3.

2.2.9 Nanshan 26-m Telescope

The Nanshan 26-m Telescope (hereafter NSRT26) has a Cassegrain-type design with a 26-m diameter main reflector and a 3-m sub-reflector on Az-El mount. The telescope was constructed in 1993 with 25-m-diameter main reflector, while refurbishment of the telescope was completed in 2015 resulting in enlargement of the main reflector of 26 m and improvement of the antenna surface accuracy. Receivers at five frequency bands, L, S/X, C, K, and Q, are equipped, while the new Q-band cooled receiver had been installed in 2018 and now is under evaluation. The C-band receiver is available for the common-use observations in the 2024A semester on a shared-risk basis. The surface accuracy of main- and sub-reflectors are 0.4 mm rms and 0.1 mm rms, respectively. The slewing rates of the main reflector are 1.0°/sec in azimuth and 0.5°/sec in elevation, as shown in Table 3.

2.2.10 Kunming 40-m Telescope

While the Kunming 40-m telescope will not be available in the 2024A semester due to the problem in the telescope driving system, detailed information is summarized in this section for references.

The Kunming 40-m Telescope (hereafter KMRT40) has a Cassegrain-type design with a 40-m diameter main reflector and a 4.2-m sub-reflector on Az-El mount. The main reflector which diameter within 26 meters is solid aluminum panel and 26 to 40 meters is stainless steel mesh. The telescope was constructed in 2006 with only S/X receivers and upgraded in 2016 for installing a C-band receiver (4–8 GHz). The surface accuracy of solid aluminum panel and stainless steel mesh are 0.5 mm rms and 2.5 mm rms, respectively. The slewing rates of the main reflector are 1.0°/sec in azimuth and 0.5°/sec in elevation, as shown in Table 3.

2.2.11 Sejong 22-m Telescope

The Sejong Telescope (hereafter KSJ) is a Cassegrain-type 22-m diameter telescope built primarily for geodetic research, and can be observed at S, X, K and Q bands. Among them, S/X bands were designed for observation with the International VLBI Service (IVS), while K- and Q bands were designed for astronomical observation. The slewing speed of the antenna is $\sim 5^{\circ}/\text{sec}$ in both azimuth and elevation, which enables fast position-switching observations (see Table 3). Like KVN telescopes, the subreflector position, tilt, and tip are remotely controlled and modeled to compensate for the gravitational deformation of the main reflector and for the sagging-down of the subreflector itself. The pointing accuracy is $\sim 3''$ and 5'' in the azimuth and elevation, respectively.

Table 3: Driving performance of EAVN telescopes.

	Table 5: Dri	ving performance of	EAVN telescopes.
Driving axis	Driving range	Max. driving speed	Max. driving acceleration
		Nobeyama	
$\overline{\mathrm{AZ}^a}$	$-75^{\circ} \sim 435^{\circ}$	$0.3^{\circ}/\mathrm{sec}$	$0.3^{\circ}/\mathrm{sec}^2$
EL	$12^{\circ} \sim 80^{\circ}$	$0.3^{\circ}/\mathrm{sec}$	$0.3^{\circ}/\mathrm{sec}^2$
		Takahagi	,
$-$ A Z^a	$11^{\circ} \sim 349^{\circ}$	$0.07^{\circ}/\text{sec}$	$0.035^{\circ}/\mathrm{sec}^2$
EL	$5^{\circ} \sim 88^{\circ c}$	$0.07^{\circ}/\mathrm{sec}$	$0.035^{\circ}/\mathrm{sec}^2$
		Hitachi	,
AZ^a	$2^{\circ} \sim 358^{\circ}$	$0.2^{\circ}/\mathrm{sec}$	$0.12^{\circ}/\mathrm{sec}^2$
EL	$5^{\circ} \sim 88^{\circ c}$	$0.2^{\circ}/\mathrm{sec}$	$0.12^{\circ}/\mathrm{sec}^2$
		Yamaguchi	,
$-$ AZ a	$2^{\circ} \sim 358^{\circ}$	$0.25^{\circ}/\mathrm{sec}$	$0.5^{\circ}/\mathrm{sec^2}$
EL	$5^{\circ} \sim 85^{\circ}$	$0.25^{\circ}/\mathrm{sec}$	$0.5^{\circ}/\mathrm{sec^2}$
		Tianma	,
$-$ AZ a	$-60^{\circ} \sim 425^{\circ}$	$0.5^{\circ}/\mathrm{sec}$	$0.27^{\circ}/\mathrm{sec}^2$
EL	$8^{\circ} \sim 88^{\circ}$	$0.3^{\circ}/\mathrm{sec}$	$0.16^{\circ}/\mathrm{sec}^2$
		Sheshan	,
$-$ AZ a	$-78^{\circ} \sim 430^{\circ}$	$1.0^{\circ}/\mathrm{sec}$	$0.5^{\circ}/\mathrm{sec}^2$
EL	$5^{\circ} \sim 88.5^{\circ}$	$0.6^{\circ}/\mathrm{sec}$	$0.28^{\circ}/\mathrm{sec}^2$
		Nanshan	,
$-$ AZ a	$-270^{\circ} \sim 270^{\circ}$	$1.0^{\circ}/\mathrm{sec}$	$0.5^{\circ}/\mathrm{sec}^2$
EL	$5^{\circ} \sim 88^{\circ}$	$0.5^{\circ}/\mathrm{sec}$	$0.5^{\circ}/\mathrm{sec}^2$
		Kunming	,
$\overline{\mathrm{AZ}^a}$	$-270^{\circ} \sim 270^{\circ}$	1.0°/sec	$0.3^{\circ}/\mathrm{sec}^2$
EL	$8^{\circ} \sim 88^{\circ}$	$0.5^{\circ}/\mathrm{sec}$	$0.3^{\circ}/\mathrm{sec^2}$
		VERA	,
$\overline{\mathrm{AZ}^a}$	$-90^{\circ} \sim 450^{\circ}$	2.1°/sec	$2.1^{\circ}/\mathrm{sec^2}$
EL	$5^{\circ} \sim 85^{\circ}$	$2.1^{\circ}/\mathrm{sec}$	$2.1^{\circ}/\mathrm{sec^2}$
FR^b	$-270^{\circ} \sim 270^{\circ}$	$3.1^{\circ}/\mathrm{sec}$	$3.1^{\circ}/\mathrm{sec^2}$
		KVN	,
$\overline{\mathrm{AZ}^a}$	$-90^{\circ} \sim 450^{\circ}$	$3.0^{\circ}/\mathrm{sec}$	$3.0^{\circ}/\mathrm{sec}^2$
EL	$5^{\circ} \sim 85^{\circ}$	$3.0^{\circ}/\mathrm{sec}$	$3.0^{\circ}/\mathrm{sec^2}$
		Sejong	,
$\overline{\mathrm{AZ}^a}$	$-270^{\circ} \sim 270^{\circ}$	5.0°/sec	$5.0^{\circ}/\mathrm{sec}^2$
EL	$0^{\circ} \sim 90^{\circ}$	$5.0^{\circ}/\mathrm{sec}$	$5.0^{\circ}/\mathrm{sec}^2$
	0° and the east		,

^aThe north is 0° and the east is 90° .

^bField rotator. FR is 0° when Beam-1 is at the sky side and Beam-2 is at the ground side, and CW is positive when a telescope is seen from a target source.

^cRecommended EL range is 15°-85° for the Takahagi and Hitachi antennas.

Table 4: Aperture efficiency, beam size, and DPFU a of EAVN telescopes.

		G-1	C-band $(6.7 GHz)$	Hz)	K-	K-band (22	GHz)		Q-band (43	GHz)
Telescope	D	η_{A}	HPBW	DPFU	η_{A}	HPBW	DPFU	η_{A}	HPBW	DPFU
Name	(m)	(%)	(arcsec)	(K/Jy)	(%)	(arcsec)	(K/Jy)	(%)	(arcsec)	(K/Jy)
Nobeyama	45				61	72	0.351	53	39	0.305
Takahagi	32				30	100	0.087			
Hitachi	32	60 - 75	270 - 280	0.197						
Yamaguchi	32	02-09	310	0.197						
Tianma	65	50 - 55	140	0.631	20	44	0.601	45	22	0.541
Nanshan	26	45 - 50	370	0.091	09	115	0.115			
Sheshan	25	40 - 42	370	0.073						
$\operatorname{Kunming}^b$	40	20 - 30	282	0.121						
Mizusawa	20	50 - 55	530	0.060	48	139	0.055	20	74	0.057
Iriki	20	50 - 55	510	0.060	44	147	0.050	40	74	0.046
Ogasawara	20	50 - 55	515	0.060	43	142	0.049	42	74	0.048
Ishigakijima	20	50 - 55	530	0.060	44	142	0.050	42	72	0.048
Yonsei	21				29	133	0.084	29	72	0.091
Ulsan	21	62	420	0.078	28	131	0.098	73	99	0.092
Tamna	21				29	131	0.084	63	89	0.080
Sejong	22				20	127	0.087	99	61	0.083
<u>a</u> . D	_	Jan -: 1	1111							

a: Degree Per Flux density Unit. b: Low η_{A} due to problems with the feed, fixing.

2.2.12 Aperture Efficiency

The aperture efficiency of each VERA antenna is 50–55% at C-band, and about 40– 50% at both K- and Q-bands (see Table 4). The measurements at C-band were based on the observations of 3C274 and Cyg-A (3C405) assuming that the flux densities are 58.7 and 237.4 Jy in C-band [17], respectively. For the K- and Q-bands, Jupiter is used for aperture efficiency measurements assuming the brightness temperature of 160 K in both K- and Q-bands. Due to the bad weather condition in some of the sessions, the measured efficiencies show large scatter. However, we conclude that the aperture efficiencies are not significantly changed compared with previous measurements. The elevation dependence of aperture efficiency for VERA antenna was also measured from the observations toward Cyg-A (3C405) and maser sources at C-band and K/Q-bands, respectively. Figure 5 (bottom-right panel) shows the relations between the elevation and the aperture efficiency measured for VERA Iriki station at K/Q-bands, while Figure 6 shows the same relation measured via integrating all the VERA stations data in C-band. The aperture efficiency at low elevation of ≤ 30 deg increases slightly in C-band, while < 20 deg decreases slightly in K/Q-bands. However, possible changes in the efficiency is less than about 20% and 10% at C- and K/Q-bands, respectively. Concerning this elevation dependence, the observing data FITS file include a gain curve table (GC table), which is AIPS readable, in order to calibrate the dependence when the data reduction.

The aperture efficiency and beam size for each KVN antenna are also listed in Table 4. Aperture efficiency of KVN varies with elevation as shown in Figure 5. The main reflector panels of KVN antennas were installed to give the maximum gain at the elevation angle of 48°. The sagging of sub-reflector and the deformation of main reflector by gravity with elevation results in degradation of antenna aperture efficiency with elevation. In order to compensate this effect, KVN antennas use a hexapod to adjust sub-reflector position. Figure 5 shows the elevation dependence of antenna aperture efficiency of the KVN 21 m radio telescopes measured by observing Mars or Jupiter. By fitting a second order polynomial to the data and normalizing the fitted function with its maximum, we derived a normalized gain curve which has the following form:

$$G_{\text{norm}} = A_0 E L^2 + A_1 E L + A_2,$$
 (1)

where EL is the elevation in degree.

Aperture efficiency and beam size for non-KaVA telescopes are also summarized in Table 4. The values for NRO45 are based on the latest measurements in autumn 2017, where the Jupiter or the Mars was used as a reference source. The elevation dependence of the aperture efficiency is approximately constant over a range of El $\sim 25^{\circ}$ – 50° at both K- and Q-bands.

In TMRT65, the main reflector panels were assembled to give the maximum surface accuracy at the elevation angle of 52° . The aperture efficiency goes down to less than 10% at low ($< 10^{\circ}$) and high ($> 80^{\circ}$) elevation angles, mainly due to the gravitational deformation. The active surface control system is used for compensating the gravitational effect at different elevation angles, making the gain curves as a constant over the elevation. Figure 7 shows the elevation dependence of the aperture efficiency at Q-band with or without the active surface control. The active surface control system is set 'ON' by default at K- and Q-band observations. To calibrate visibility amplitude, conversion factors from temprature (in unit of K) to flux density (in unit of Jy) are

required. These factors, DPFU (Degree Per Flux density Unit), are also summarized in Table 4.

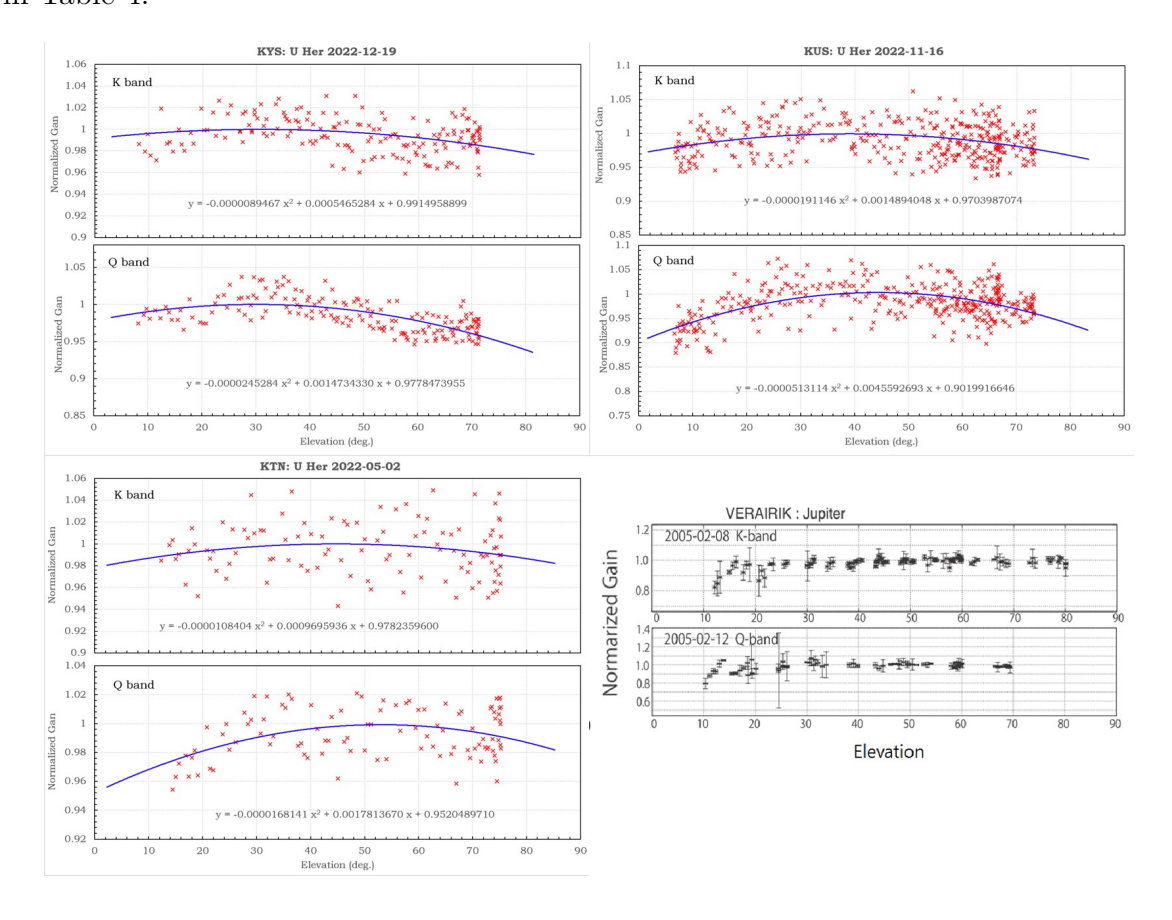


Figure 5: The elevation dependence of the aperture efficiency for KVN three antennas and VERA Iriki antenna. The efficiency in K-band (on Feb 8, 2005) and the Q-band (on Feb 12, 2005) for VERA Iriki antenna is shown in *bottom right*. The efficiency is relative value to the measurement at $EL = 50^{\circ}$.

2.2.13 Beam Pattern and Size

Figure 8 upper panels shows the beam patterns for VERA at K-band. The side-lobe level is less than about -15 dB, except for the relatively high side-lobe level of about -10 dB for the separation angle of 2.0 deg at Ogasawara station. The side-lobe of the beam patterns has an asymmetric shape, but the main beam has a symmetric Gaussian shape without dependence on separation angle. Figure 9 shows the beam patterns for VERA Mizusawa and Ishigakijima stations at C-band (single-beam mode) measured via observing strong CH₃OH maser sources G 009.62+00.196 and W3-IRS5, which can be assumed as a point source, on 2017 Apr 5-8. Almost the similar side-lobe pattern is clearly seen in both stations and other VERA two stations as well. The measured beam sizes (HPBW) in C-, K- and Q-bands based on the data of the pointing calibration are also summarized in Table 4. The main beam sizes show no dependence on the dual-beam separation angle.

The optics of KVN antenna is a shaped Cassegrain type of which the main reflector and subreflector are shaped to have a uniform illumination pattern on an aperture plane. Because of the uniform illumination, KVN antennas can get higher aperture

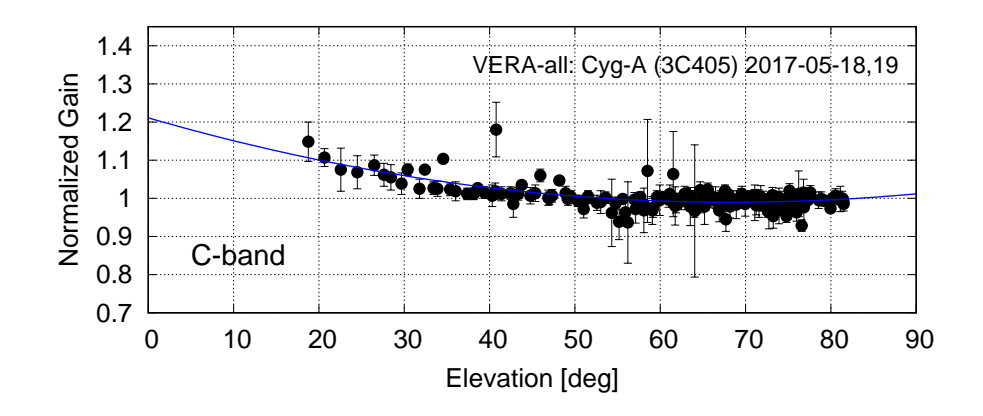


Figure 6: The elevation dependence of the aperture efficiency for VERA in C-band. This gain curve was measured on May 18 and 19, 2017 via observing Cyg-A (3C405) and integrating all the VERA stations data. The efficiency in this plot is relative value to the measurement at $EL = 50^{\circ}$.

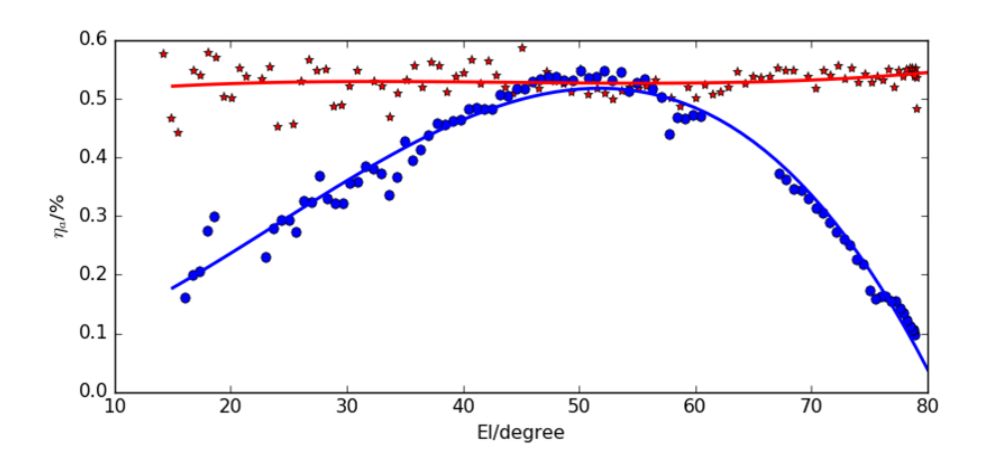


Figure 7: The elevation dependence of the aperture efficiency ($\eta_{\rm eff}$) for TMRT65 at Q-band. The red and blue colors represent $\eta_{\rm eff}$ with or without the active surface control, respectively.

efficiency than value of typical Cassegrain type antenna. However, higher side-lobe level is inevitable. OTF images of Jupiter at K- and Q-bands are shown in Figure 8. The map size is $12' \times 10'$ and the first side-lobe pattern is clearly visible. Typical side-lobe levels of KVN antennas are 13–14 dB.

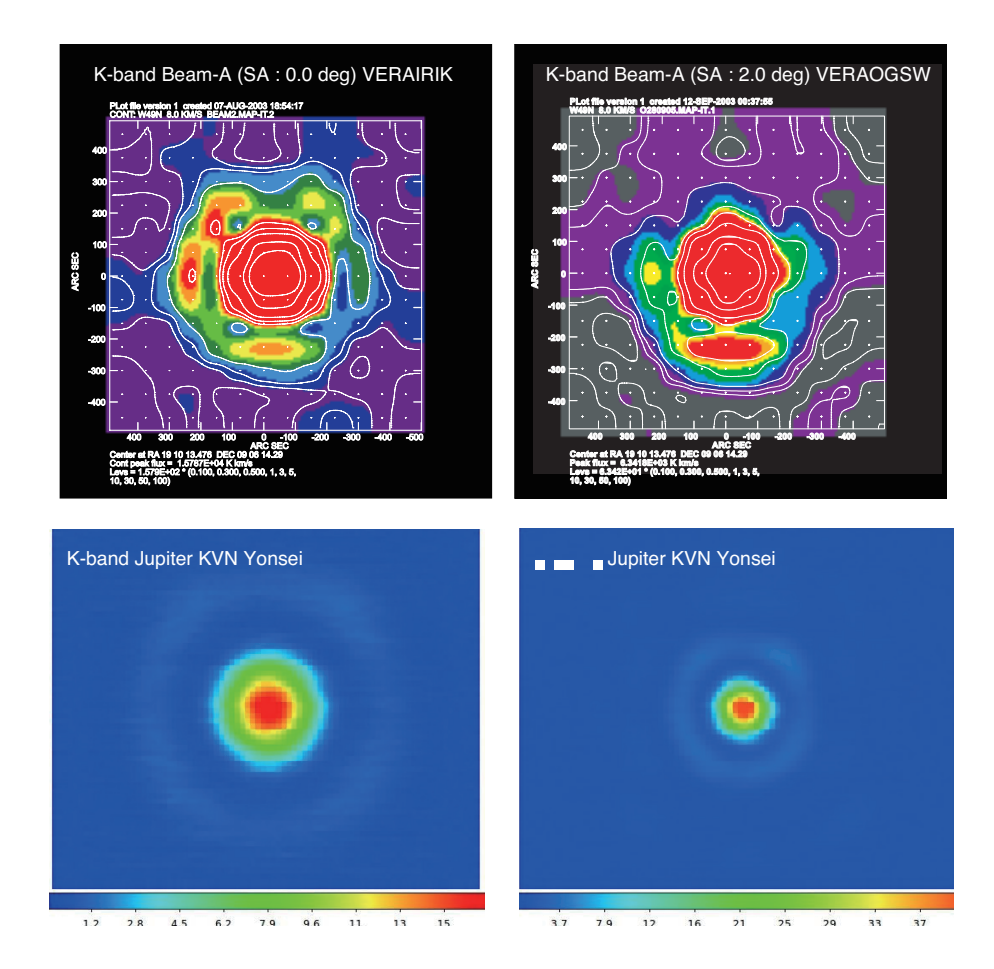


Figure 8: The beam patterns in the K-band for VERA (A-beam) Iriki with the separation angle of 0° (*Upper left*) and Ogasawara with the separation angle of 2.0° (*Upper right*), and in K/Q-band for KVN Yonsei. The patterns of VERA antennas were derived from the mapping observation of strong H₂O maser toward W49N, which can be assumed as a point source, with grid spacing of 75". In the case of KVN antennas, the patterns were derived from the OTF images of Venus at K/Q-band.

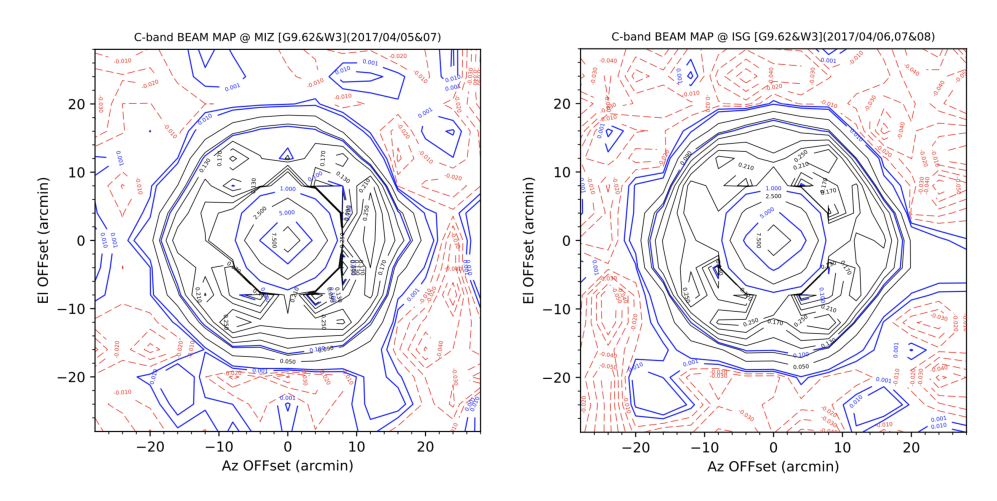


Figure 9: The beam patterns in C-band for VERA antennas (single beam) at Mizusawa and Ishigakijima stations. The patterns were derived from the mapping observation of strong CH₃OH masers toward G 009.62+00.196 and W3-IRS5, which can be assumed as a point source, with grid spacing of 4' in $56' \times 56'$ field. These observations were done in Apr 5–8, 2017.

2.3 Receivers

2.3.1 Brief Summary of VERA Receiving System

Each VERA antenna has the receivers for 5 bands, which are S (2 GHz), C (6.7 GHz), X (8 GHz), K (22 GHz), and Q (43 GHz) bands. For the open use, C-band, K-band and Q-band are open for observation in the single-polarization (LCP) mode. Observations of the dual-circular-polarization are also available for open use programs at K- and Q-bands on a risk-shared basis. The low-noise HEMT amplifiers in the K- and Q-bands are enclosed in the cryogenic dewar, which is cooled down to 20 K, to reduce the thermal noise. On the other hand, both the amplifier and polarizer in C-band are operated at room temperatures. The range of observable frequency and the typical receiver noise temperature $(T_{\rm RX})$ at each band are summarized in Table 5 and Figure 10.

Table 5: Frequency range and T_{RX} of receivers at each EAVN telescope.

Band	Frequency Range	$\frac{d T_{RX} d T_{RX}}{T_{RX}^a}$	Polarization
	[GHz]	[K]	
	[]	Nobeyam	a.
K	21.5 - 23.8	~ 85	LCP/RCP
Q	42.5 - 44.5	~ 111	LCP
		Takahag	i
K	21.0 - 25.0	~ 30	LCP/RCP
		Hitachi	·
С	6.6 - 7.1	~ 20	LCP/RCP
		Yamagucl	ni
С	6.6 - 7.1	18	LCP/RCP
		Tianma	
С	4.0 - 8.0	~ 20	LCP/RCP
K	18.0 - 26.5	16 - 35	LCP/RCP
Q	39 - 47	35 - 50	LCP/RCP
		Nanshan	
С	4.0 - 8.0	~ 15	LCP/RCP
K	22.0 - 24.2	~ 15	LCP/RCP
Q		(under ev	aluation)
		Sheshan	
С	5.975 - 6.825	~ 100	LCP/RCP
		Kunming	
С	4.0 - 8.0	~ 20	LCP/RCP
		VERA	
С	6.3 - 7.0	80 - 100	LCP
K	21.5 - 23.8	30 - 50	LCP/RCP^c
Q	42.5 - 44.5	70 - 90	LCP/RCP
		KVN	
C^{b}	6.3 - 7.0	~ 300	LCP
K	18 - 26	20 - 40	LCP/RCP
Q	35 - 50	50 - 80	LCP/RCP
		Sejong	T 000 /T 000
K	21.4 - 23.1	~ 31	LCP/RCP
Q a D	42.3 – 43.9	~ 86	LCP/RCP

^a Receiver noise temperature.

After the radio frequency (RF) signals from astronomical objects are amplified by the receivers, the RF signals are mixed with standard frequency signal generated in the

^b Only for the Ulsan antenna.

 $^{^{}c}$ RCP is used for the simultaneous K/Q band mode (see Section 4.5).

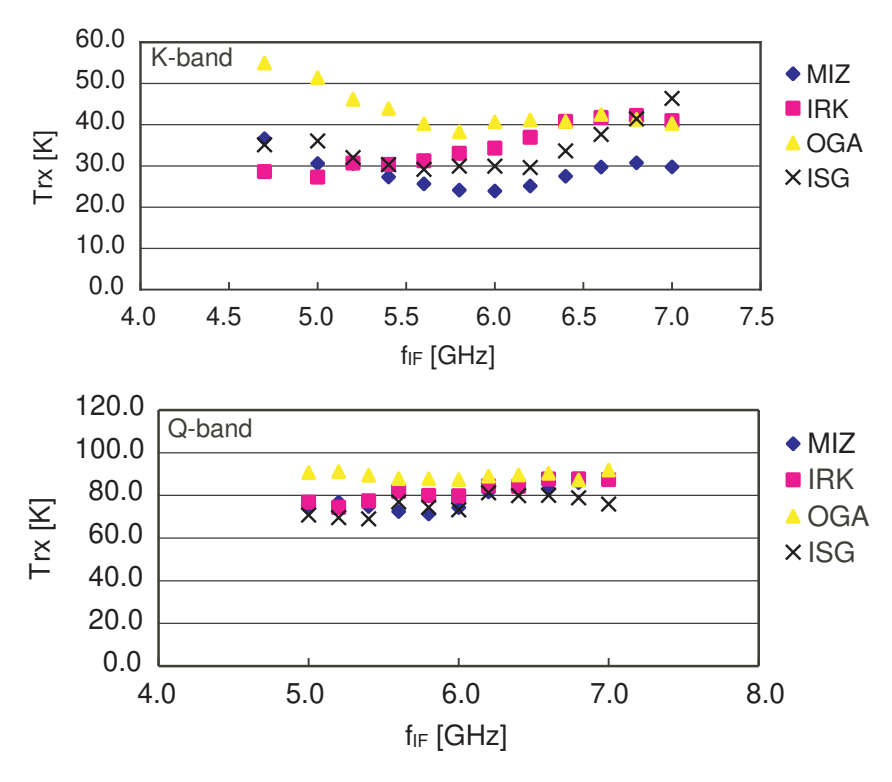


Figure 10: Receiver noise temperature for each VERA antenna. Top and bottom panels show measurements in the K- and Q-bands, respectively. Horizontal axis indicate an IF (intermediate frequency) at which $T_{\rm RX}$ is measured. To convert it to RF (radio frequency), add 16.8 GHz in K-band and 37.5 GHz in Q-band to the IF frequency.

first local oscillator to down-convert the RF to an intermediate frequency (IF) of 4.7 – $7~\mathrm{GHz}$. The first local frequencies are fixed at $16.8~\mathrm{GHz}$ in K-band and at $37.5~\mathrm{GHz}$ in Q-band. The IF signals are then mixed down again to the base band frequency of $0-512~\mathrm{MHz}$. The frequency of second local oscillator is tunable with a possible frequency range between $4~\mathrm{GHz}$ and $7~\mathrm{GHz}$. The correction of the Doppler effect due to the earth rotation is carried out in the correlation process after the observation. Therefore, basically the second local oscillator frequency is kept to be constant during the observation. Figure 11 shows a flow diagram of these signals for VERA.

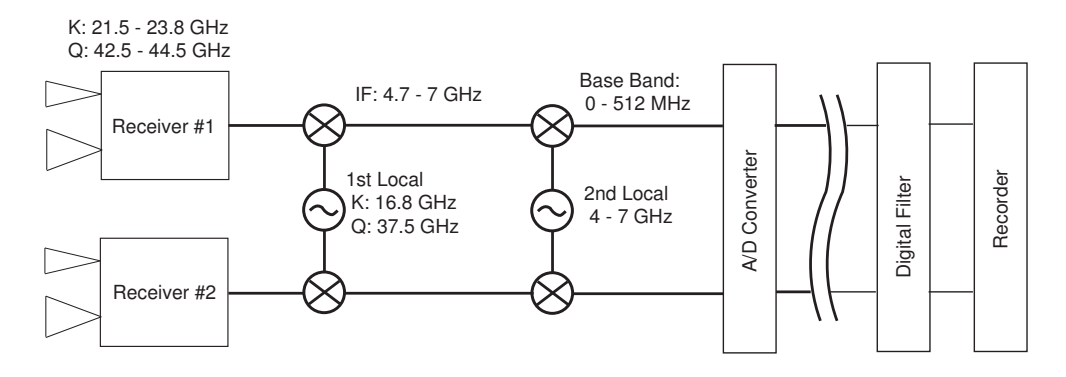


Figure 11: Flow diagram of signals from receiver to recorder for VERA.

2.3.2 Brief Summary of KVN Receiving System

The KVN quasi-optics are uniquely designed to observe 22, 43, 86 and 129 GHz band simultaneously [7], [8]. Figure 12 shows the layout of quasi-optics and receivers viewing from sub-reflector side. The quasi-optics system splits one signal from sub-reflector into four using three dichroic low-pass filters marked as LPF1, LPF2 and LPF3 in the Figure 12. The split signals into four different frequency bands are guided to corresponding receivers.

Figure 13 shows a signal flows in KVN system. The 22, 43 and 86 GHz band receivers are cooled HEMT receivers and the 129 GHz band receiver is a SIS mixer receiver. All receivers can receive dual-circular-polarization signals. The dual-circular-polarization mode is available for open use programs at K- and Q-bands on a risk-shared basis. Among eight signals (four dual-polarization signals), four signals selected by the IF selector are down-converted to the input frequency band of the sampler. The instantaneous bandwidth of the 1st IF of each receiver is limited to 2 GHz by the band-pass filter. The 1st IF signal is down-converted by BBCs to the sampler input frequency (512 – 1024 MHz) band.

Typical noise temperatures of K- and Q-bands are presented in Table 5. Since the calibration chopper is located before the quasi-optics as shown in Figure 12, the loss of quasi-optics contributes to receiver noise temperature instead of degrading antenna aperture efficiency. Therefore, the noise temperature in the table includes the contribution due to the quasi-optics losses.

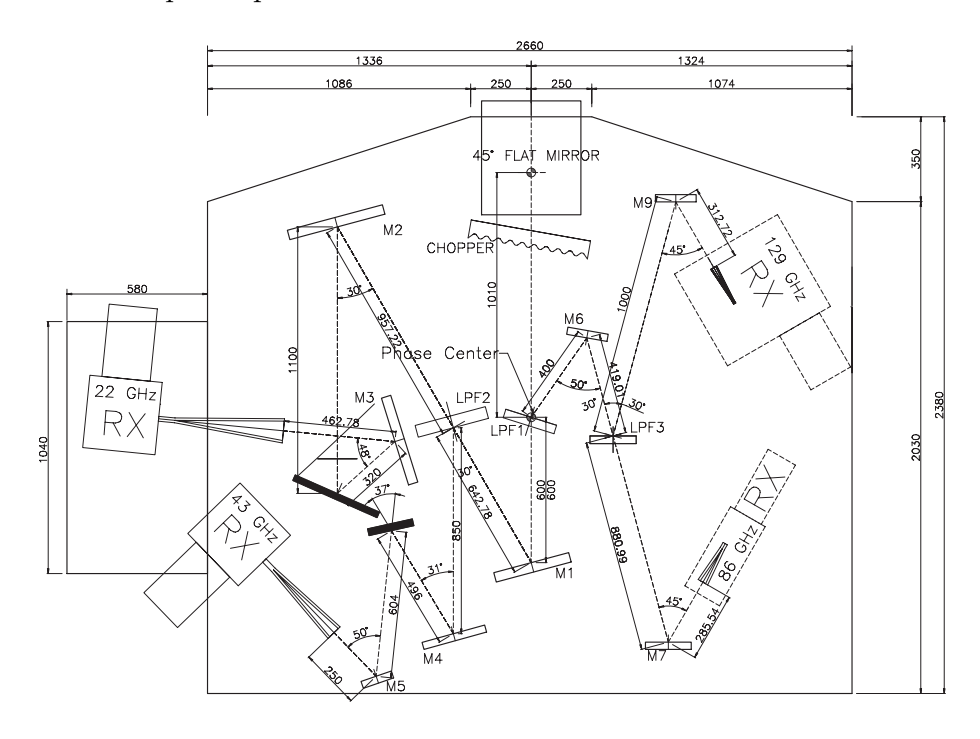


Figure 12: KVN multi-frequency receiving system [7], [8].

2.3.3 Brief Summary of NRO45 Receiving System

While the Nobeyama 45 m telescope will not be available in the 2024A semester due to the problem in the hydrogen maser operated by the Mizu-

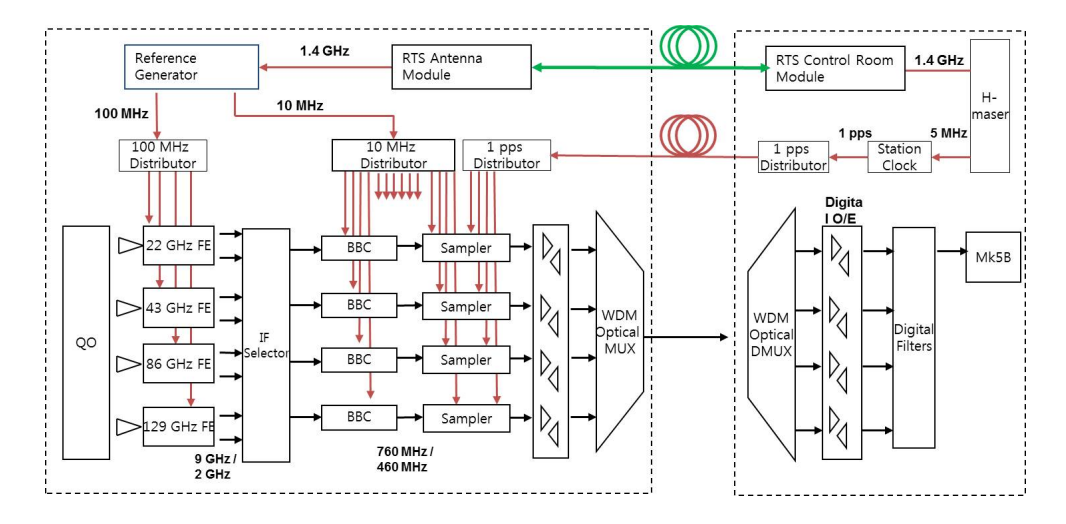


Figure 13: Flow diagram of signals from receiver to recorder for KVN [15].

sawa VLBI Observatory of NAOJ, detailed information is summarized in this section for references.

The NRO45 covers an observing frequency range of 20 – 116 GHz with multiple receivers. The VLBI backend system of the NRO45 is currently equipped at K-band and Q-band. Figure 14 illustrates a flow diagram of the VLBI receiving system in the NRO45. The observable RF range and typical receiver noise temperature for the receivers at K- and Q-bands are also summarized in Table 5. The received RF signals are down-converted into an IF range of 5 – 7 GHz, then the IF signals are mixed down to the another IF range of 400–2000 MHz, and finally filtered to the base bands of 512 –1024 MHz and 1024–1536 MHz in K- and Q-bands, respectively, which are the inputs to the A/D sampler. Because of the fixed frequencies of the first (16800 MHz) and second (4500 MHz) local oscillators and the bandpass filter (512–1024 MHz), the frequency range of the RF signal is fixed to 21812–22324 MHz for K-band. Only LCP signals are recorded in both K-band and Q-band (except for simultaneous K/Q band mode).

By default, one of the receivers at K- or Q-band can be selected by switching the mirrors in the optics in a few minutes manually. Since 2020B, K- and Q-band observations can be conducted simultaneously by inserting a perforated high-pass dichroic plate [16]. When using the dichroic plate, the gain of the Q-band signals may be reduced by 0.3 dB (in 2018 June), causing the rise of the system noise temperature by about 30 K in Q-band. In the case of the simultaneous K- and Q- band observations, RCP and LCP signals are recorded, respectively (See Table 26).

2.3.4 Brief Summary of TAK32 Receiving System

Figure 15 shows a flow diagram of the VLBI receiving system in TAK32. TAK32 covers an observing frequency range of 6-9 GHz and 21-25 GHz with two cryogenically-cooled receivers, while TAK32 joins in EAVN observations at only K-band in the 2024A semester.

The flow diagram of TAK32 is shown in Figure 15. The K-band receiver is cooled with dual circular polarization. Observations of both single- (LCP) and dual-circular-

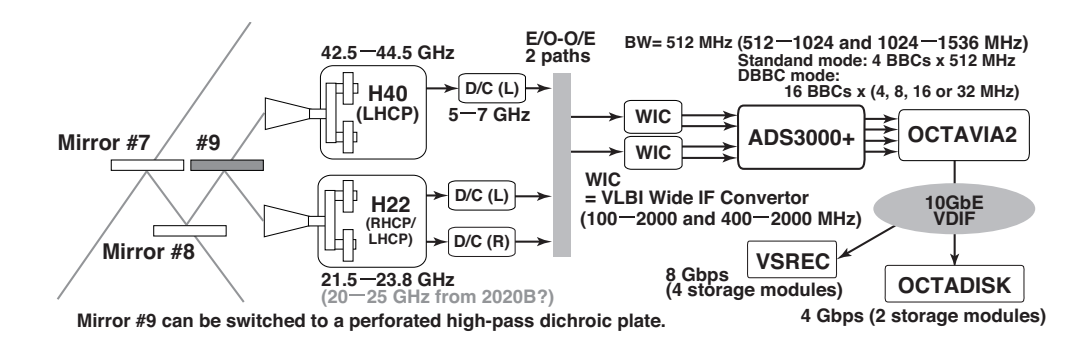


Figure 14: Flow diagram of signals from receiver to recorder for NRO45.

polarization are available for the EAVN open use while the latter will be conducted on a risk-shared basis. The observable frequency range and the typical receiver noise temperature are shown in Table 5. The total system noise temperatures at K-band is typically 40 K at winter with good weather, > 100 K at winter with bad weather, 150 K at summer with good weather, and > 500 K at summer with bad weather.

For K-band, received RF signals are down-converted into an IF range of 8.0-8.8 GHz, and the IF signals are then mixed down to the base band of 512-1024 MHz, which is the input to the A/D sampler ADS-3000+. The data with the rate of 1024 MHz \times 2 bit are recorded by OCTADISK, and then the digital base-band converter is used to convert the 2 Gbps data into 1 Gbps.

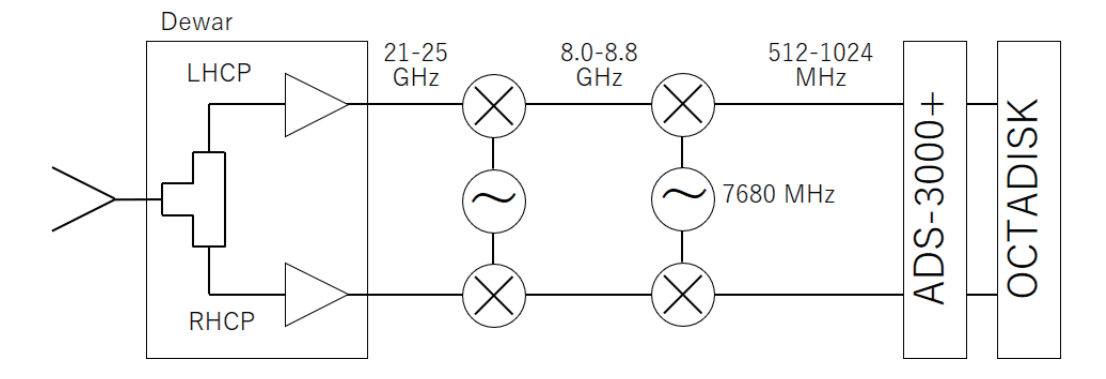


Figure 15: Flow diagram of signals from receiver to recorder for TAK32.

2.3.5 Brief Summary of HIT32 Receiving System

Figure 16 shows a flow diagram of the VLBI receiving system in HIT32. HIT32 covers an observing frequency range of 6-9 GHz and 21-25 GHz with two cryogenically-cooled receivers, while HIT32 joins in EAVN observations at only C-band in the 2024A semester.

The flow diagram of HIT32 is shown in Figure 16. The C-band receiver is cooled with dual circular polarization. The observable frequency range and the typical receiver noise temperature are shown in Table 5. The total system noise temperatures at C-band is typically 30 K with good weather and ~ 40 K with bad weather.

For C-band, received RF signals are mixed down to the base band of 512 – 1024 MHz,

which is the input to the A/D sampler ADS-3000+. The data with the rate of 1024 MHz \times 2 bit are recorded by OCTADISK, and then the digital base-band converter is used to convert the 2 Gbps data into 1 Gbps.

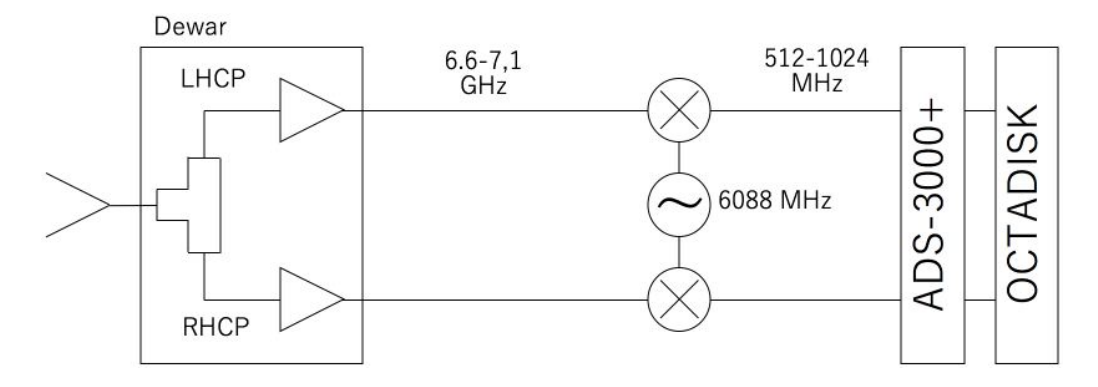


Figure 16: Flow diagram of signals from receiver to recorder for HIT32.

2.3.6 Brief Summary of YAM32 Receiving System

The flow of the VLBI receiving system in YAM32 is the same with that of HIT32. YAM32 covers an observing frequency range of 6-9 GHz with a cryogenically-cooled receivers, while YAM32 joins in EAVN observations at only C-band in the 2024A semester.

The C-band receiver is cooled with dual circular polarization. The observable frequency range and the typical receiver noise temperature are shown in Table 5. The total system noise temperatures at C-band is typically 50 K with good weather and ~ 80 K with bad weather.

For C-band, received RF signals are mixed down to the base band of 512-1024 MHz, which is the input to the A/D sampler ADS-3000+. The data with the rate of 1024 MHz \times 2 bit are recorded by OCTADISK, and then the digital base-band converter is used to convert the 2 Gbps data into 1 Gbps.

2.3.7 Brief Summary of TMRT65 Receiving System

Figure 17 shows a flow diagram of the VLBI receiving system in TMRT65. TMRT65 has the receivers for 8 frequency bands, L (1.4 GHz), S/X (2.3/8.4 GHz), C (6.7 GHz), X/Ka (8.4/31.0 GHz), Ku (15 GHz), K (22 GHz), and Q (43 GHz). The K- and Q-band receivers are cooled HEMT receivers with dual circular polarizers. The dual-circular-polarization mode is available for open use programs at K- and Q-bands on a risk-shared basis. The observable frequency range and the typical receiver noise temperature are shown in Table 5. The total system noise temperatures at K- and Q-bands are typically 70 and 110 K, respectively. The RF signal is firstly down-converted to IF range of 4-12 GHz and it is transferred by optical fibers to the observing room, where the signal is further down-converted to 0-1024 MHz (actually in 10-512 MHz and 512-1024 MHz) at the input of BBCs.

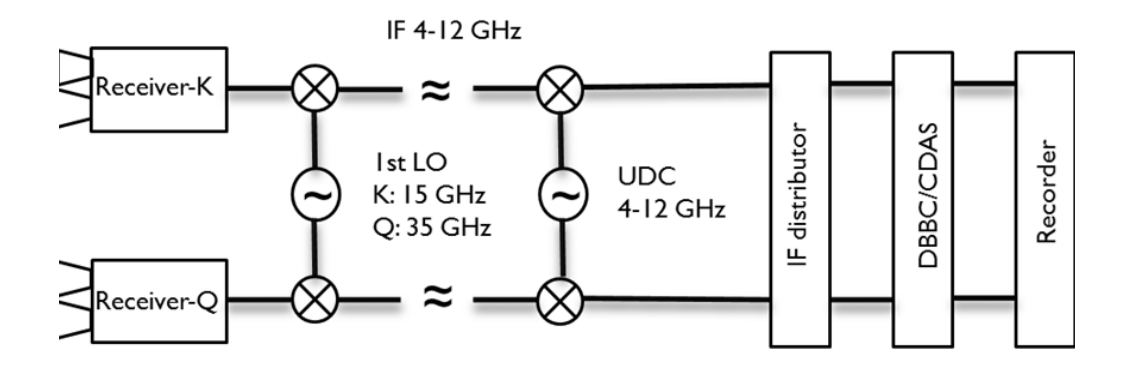


Figure 17: Flow diagram of signals from receiver to recorder for TMRT65.

2.3.8 Brief Summary of SHRT25 Receiving System

The details will be available upon request. Please contact with the EAVN User Support Team if you need further information.

2.3.9 Brief Summary of NSRT26 Receiving System

Figure 18 shows a flow diagram of the VLBI receiving system in NSRT26 at K-band. NSRT26 has the receivers for 5 frequency bands, L $(1-2\,\mathrm{GHz})$, S/X $(2.3/8.4\,\mathrm{GHz})$, C $(4-8\,\mathrm{GHz})$, K $(22\,\mathrm{GHz})$, and Q $(43\,\mathrm{GHz})$, while NSRT26 will join in EAVN observations at C-band and K-band in the 2024A semester. The C-band receiver is newly available for the common-use observations from the 2024A semester on a shared-risk basis. The C- and K-band receivers are cooled HEMT receivers with dual circular polarizers. Dual-circular-polarization mode is available at the C- and K-bands for open use programs on a risk-shared basis. The observable frequency range and the typical receiver noise temperature are shown in Table 5. The total system noise temperatures at C- and K-bands are typically 50 and 42 K, respectively. The C-band RF signal is down-converted straightly to IF range of $70-1024\,\mathrm{MHz}$ while the K-band RF signal is down-converted with three stages to IF range of $100-600\,\mathrm{MHz}$. The analog-digital conversion and digital filtering of the IF signal for both C- and K-bands are conducted using either the Digital Baseband Converter 2 (DBBC2) system or the Chinese VLBI Data Acquisition System 2 (CDAS2).

2.3.10 Brief Summary of KMRT40 Receiving System

While the Kunming 40 m telescope will not be available in the 2024A semester due to the problem in the telescope driving system, detailed information is summarized in this section for references.

Figure 19 shows a flow diagram of the VLBI receiving system in KMRT40. KMRT40 has the receivers for 3 frequency bands, S/X (2.2/8.4 GHz), C (4–8 GHz, Lo is tuneable), while KMRT40 joins in EAVN observations at only C-band in the EAVN sessions. The C-band receiver is an HEMT cooled receiver with dual circular polarizations. The observable frequency range and the typical receiver noise temperature are shown in Table 5. The total system noise temperatures at C-band is typically 20 K. The RF signal is down-converted with three stages, and analog-digital conversion and digital

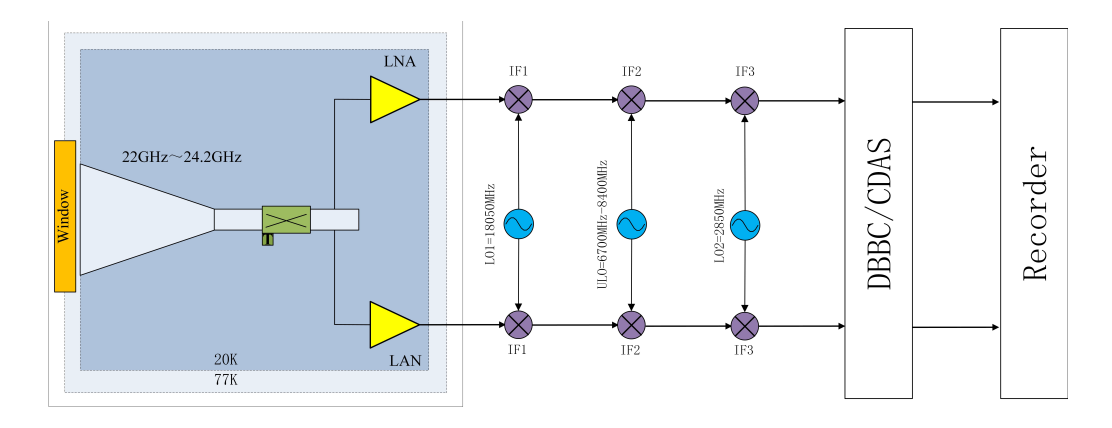


Figure 18: Flow diagram of signals from receiver to recorder for NSRT26 at K-band.

filtering of the IF signal is conducted using either the Digital Baseband Converter 2 (DBBC2) system or the Chinese VLBI Data Acquisition System 1 (CDAS1).

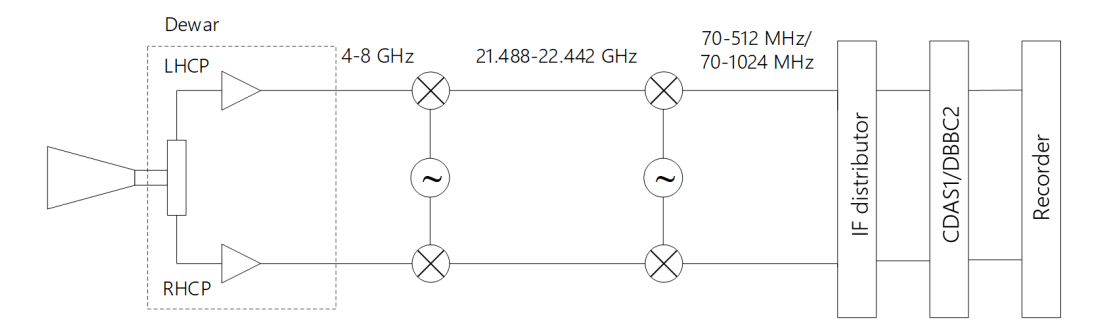


Figure 19: Flow diagram of signals from receiver to recorder for KMRT40.

2.3.11 Brief Summary of KSJ Receiving System

The KSJ antenna has the capability to observe four bands, which are S (2 GHz), X (8 GHz), and simultaneous K/Q (22/43 GHz) bands. Figure 20 shows the layout of quasi-optics and receivers. During the 2024A semester of EAVN observation, only K- and Q- bands are available. For VLBI performance at 22 and 43 GHz, the KSJ telescope was equipped with the the same LPF used in the KVN telescope, so the receiver noise temperature was significantly improved, indicating \sim 31 K at 22 GHz and \sim 86 K at 43 GHz.

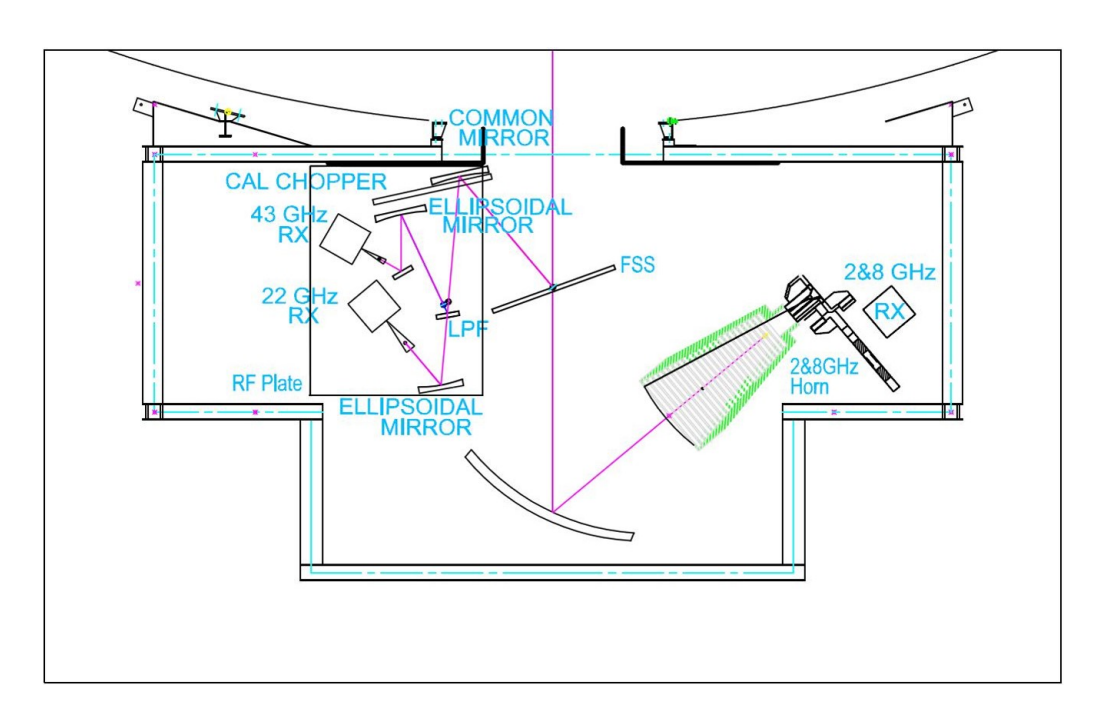


Figure 20: The KSJ quasi-optics and receiving system

2.4 Digital Signal Processing

In VERA system, A/D (analog-digital) samplers convert the analog base band outputs of 0-512 MHz \times 2 beams to digital form. The A/D converters carry out the digitization of 2-bit sampling with the bandwidth of 512 MHz and the data rate is 2048 Mbps for each beam.

In KVN system, A/D samplers digitize signals into 2-bit data streams with four quantization levels. The base band output is 512 – 1024 MHz. The sampling rate is 1024 Mega sample per second (Msps) with 2-bit sampling, resulting in the data rate of 2 Gbps at the frequency bandwidth of 512 MHz. Four streams of 512 MHz band width (2 Gbps data rate) can be obtained in the KVN multi-frequency receiving system simultaneously, which means that the total rate is 8 Gbps. In KSJ system, K5 and DBBC3 system are available. The maximum supported data rates of K5 and DBBC3 systems are 1 and 8 Gbps with a 2-bit sampling. With K5 and DBBC3 systems, a simultaneous observing mode of S/X and K/Q bands are supported by the KSJ quasi-optics (Figure 20).

In NRO45 (K-band), TAK32, HIT32, and YAM32 systems, the baseband signal output is 512-1024 MHz and the A/D samplers perform 2-bit digitization with four quantization levels. A maximum recording rate of 2048 Mbps is possible with a total bandwidth of 512 MHz. In NRO45 Q-band, the baseband signal output is 1024-1536 MHz.

Since the total data recording rate is limited to 1024 Mbps (see the next section), only part of the sampled data can be recorded onto hard disks. The data rate reduction is done by a digital filter system, with which one can flexibly choose number and width of recording frequency bands.

Observers can select modes of the digital filter listed in the Table 6. In VERA7SIOS mode in the Table 6, two transitions (v=1 & 2) of SiO maser in the Q band can be simultaneously recorded.

When VERA performs the K/Q-band simultaneous observation, GEO1D mode should be selected. Because the common second local oscillator (local frequency $\nu_{\rm BBCLO}$) are used for both K-band and Q-band, the local frequencies in these bands, $\nu_{\rm RF,22~GHz}$ and $\nu_{\rm RF,43~GHz}$ shall be linked as follows:

$$\nu_{\text{RF,22 GHz}} = \nu_{\text{1st-LO,22 GHz}} + \nu_{\text{BBCLO}} \tag{2}$$

$$\nu_{\text{RF,43 GHz}} = \nu_{\text{1st-LO,43 GHz}} + \nu_{\text{BBCLO}} \tag{3}$$

Here $\nu_{\rm 1st-LO,22~GHz}$ =16800 MHz and $\nu_{\rm 1st-LO,43~GHz}$ =37500 MHz are fixed. Under this constraint, the K/Q-band simultaneous observation with VERA and NRO45 shall cover the RF frequencies of 21812–22324 MHz (see Section 2.3.3) and 42512–43024 MHz at K-band and Q-band, respectively.

For 1 Gbps dual-polarization recording, either GEO1D ($16\,\mathrm{MHz} \times 8$ channels \times 2 polarizations) or VERA4D ($32\,\mathrm{MHz} \times 4$ channels \times 2 polarizations) must be selected. See Table 7.

2.5 Recorders

The EAVN observations are basically limited to record with 1024 Mbps data rate. VERA, NRO45, TAK32, HIT32, and YAM32 have OCTADISK. KVN, TMRT65/SHRT25,

NSRT26, and KMRT40 use the Mark5B recording systems. KSJ use the Mark6 recording system. OCTADISK and Mark5B are hard disk recording systems developed at NAOJ and Haystack observatory, respectively. The total bandwidth is 256 MHz.

2.5.1 Note on the Data Storage Capacity

The data for all EAVN observation are recorded using OCTADISK/Mark-5B/Mark-6 data recorder depending on the station. EAVN observation data are usually recorded with the data rate of 1 Gbps, while part of observations (e.g., multi-frequency data recording mode at some of EAVN stations) are conducted using higher data sampling rate of greater than or equal to 2 Gbps. This may give rise to shortage of disk space. If it happens, EAVN operation team may ask PI of each EAVN observation to accept revision of the planned observing schedule.

2.6 Correlators

The correlation process is carried out by a VLBI correlator located at KJCC (Korea-Japan Correlation Center) at Daejeon, which has been developed as the KJJVC (Korea-Japan Joint VLBI Correlator) located at KJCC. Hereafter it is tentatively called "Daejeon correlator". Specification of The Daejeon correlator is summarized in Table 8. The Daejeon correlator can process the data stream of up to 8192 Mbps from maximum 16 antenna stations at once. Currently the raw observed data of KVN, TMRT65/SHRT25, NSRT26, and KMRT40 stations are recorded and playbacked with Mark5B, and those of VERA, NRO45, TAK32, HIT32, and YAM32 are recorded and playbacked with OC-TADISK at the data rate of 1024 Mbps. For KaVA, data formats available in 2024A are 16 IFs \times 16 MHz ("C5 mode" in The Daejeon correlator terminology), 8 IFs \times 32 MHz (C4 mode), and 2 IFs \times 128 MHz (C2 mode). For EAVN (including non-KaVA telescopes), available data formats are 16 IFs × 16 MHz (C5 mode) at C- and K-band, and 8 IFs \times 32 MHz (C4 mode) at all the C-, K- and Q-bands. Note that the C2 mode is available at only KaVA 7 telescopes because other EAVN telescopes are not equipped with the backend system for the C2 mode. Minimum integration times (time resolution) are 0.2048, 0.8192, and 1.6384 seconds for C2, C4, and C5 modes, respectively, and the number of frequency channels within each IF is 8192 for both modes (i.e. maximum frequency resolution is about 1.95 kHz). By default, the number of frequency channels is reduced to 128 (for continuum) or 512 (for line) via channel integration after correlation. One may put a special request of number of frequency channels to take better frequency resolution. The number of frequency channels can be selected among 512, 1024, 2048, 4096 or 8192. Note that we recommend the maximum frequency channel of 8192 with the C5 mode in the case of CH₃OH maser observations at C-band to achieve sufficient channel and velocity resolution at IF5 (corresponding to 6,664–6,680 MHz. Final correlated data is served as FITS-IDI file.

For the dual-polarization mode at K and Q bands, KJCC currently supports correlation of dual-polarization data up to 8 stations.

2.6.1 Note for the C2 Mode

To obtain the accurate amplitude values across the all IF channels, however, it is better to reduce the number of baseband (or IFs in data handling with AIPS) yielded by the

Table 6: Digital filter mode for EAVN.

Mode	Rate		BW/CH^b		Freq. range d		Note for spectral line
Name	(Mbps)	CH^a	(MHz)	CH^c	(MHz)	Band^e	
GEO1K*	1024	16	16	1	0 - 16	U	
0.20				$\overline{2}$	32 - 48	Ü	
				3	64 - 80	Ü	
				4	96 - 112	Ü	
				5	128 - 144	U	
				6	160 - 176	U	
				7	192 - 208	Ü	
				8	224 - 240	Ü	
				9	256 - 272	Ü	Target line (e.g. $H_2O)^f$
				10	288 - 304	Ü	(:.a. ==2 :)
				11	320 - 336	Ŭ	
				12	352 - 368	Ü	
				13	384 - 400	Ü	
				14	416 - 432	Ü	
				15	448 - 464	Ü	
				16	480 - 496	Ü	
GEO1S*	1024	16	16	1	112 - 128	L	
GEOIS	1021	10	10	2	128 - 144	U	
				3	144 - 160	Ĺ	
				4	160 - 176	U	
				5	176 - 192	L	CH ₃ OH $(J=5_1-6_0 A^+)^f$
				6	192 - 208	U	0113011 (5 - 51 - 50 71)
				7	208 - 224	L	
				8	224 - 240	U	
				9	240 - 256	L	
				10	256 - 272	U	Target line (e.g. $H_2O)^f$
				11	272 - 288	L	rarget line (e.g. 11 ₂ O)
				$\frac{11}{12}$	288 - 304	U	
				13	304 - 320	L	
						U	
				14 15	320 - 336	L	
					336 - 352	U	
VED A 7CIOC*	1094	16	1.6	16	352 - 368		
VERA7SIOS*	1024	16	16	1	32 - 48	U	
				2	64 - 80	U	C:O (I 10 2)
				3	80 - 96	L	SiO $(J=1-0, v=2)$
				4	96 - 112	U	
				5	128 - 144	U	
				6	160 - 176	U	
				7	192 - 208	U	
				8	224 - 240	U	
				9	256 - 272	U	
				10	288 - 304	U	0:0 (T 10 1)
				11	384 - 400	U	SiO $(J=1-0, v=1)$
				12	320 - 336	U	
				13	352 - 368	U	
				14	416 - 432	U	
				15	448 - 464	U	
				16	480 - 496	U	

Table 6: Digital filter mode for EAVN — continued.

Mode	Rate		$\overline{\mathrm{BW/CH}^b}$		Freq. range $\frac{1}{4}$	Side	Notes for spectral line
Name	(Mbps)	CH^a	(MHz)	CH^c	(MHz)	Band^e	
VERA4S*	1024	8	32	1	128 - 160	U	
				2	160 - 192	${ m L}$	
				3	192 - 224	U	
				4	224 - 256	${ m L}$	
				5	256 - 288	U	
				6	288 - 320	${ m L}$	
				7	320 - 352	U	
				8	352 - 384	${ m L}$	
VERA1S*	1024	2	128	1	128 - 256	L	
				2	256 - 384	U	
VERA1**	1024	2	128	1	256 - 384	U	A-Beam
,				2	256 - 384	Ü	B-Beam
VERA7**	1024	16	16	1	256 - 272	U	A-Beam for target line
, 22011,	1021	10	10	2	128 - 144	Ü	B-Beam (CH 2-16)
				3	144 - 160	Ĺ	2 2 com (cm 2 10)
				4	160 - 176	U	
				5	176 - 192	Ĺ	
				6	192 - 208	U	
				7	208 - 224	Ĺ	
				8	224 - 240	U	
				9	240 - 256	Ĺ	
				10	256 - 272	U	
				11	272 - 288	Ĺ	
				12	288 - 304	U	
				13	304 - 320	Ĺ	
				14	320 - 336	U	
				15	336 - 352	Ĺ	
				16	352 - 368	U	
VERA7MM**	1024	16	16	1	256 - 272	U	A-Beam for target line
, 23(31,1,11,1	1021	10	10	2	32 - 48	Ü	B-Beam (CH 2-16)
				3	64 - 80	Ü	()
				4	96 - 112	Ü	
				5	128 - 144	Ü	
				6	160 - 176	Ü	
				7	192 - 208	Ü	
				8	224 - 240	Ŭ	
				9	256 - 272	Ü	
				10	288 - 304	Ü	
				11	320 - 336	Ü	
				12	352 - 368	Ü	
				13	384 - 400	Ü	
				14	416 - 432	Ü	
				15	448 - 464	Ü	
				16	480 - 496	Ü	
* All channels	C A	D	(VEDA)				

^{*} All channels are for A-Beam (VERA) and LCP (EAVN).
** Mode for the phase referencing (see section 4.2).

^a Total number of channels

 $[^]b$ Bandwidth per channel in MHz

^c Channel number

^d Filtered frequency range in the base band (MHz)
^e Side Band (LSB/USB)

 $[^]f$ The total local frequency (i.e., RF frequency corresponding to IF = 0 MHz) is 21,971 MHz at K-band for GEO1K and GEO1S, and 6,488 MHz at C-band for GEO1S.

Table 7: Digital filter mode for EAVN dual polarization

Mode	Rate		BW/CH^b		Freq. range d		Polarization
Name	(Mbps)	CH^a	(MHz)	CH^c	(MHz)	Band^e	
GEO1D*	1024	16	16	1	240 - 256	L	RCP
				2	240 - 256	L	LCP
				3	256 - 272	U	RCP
				4	256 - 272	U	LCP
				5	272 - 288	${ m L}$	RCP
				6	272 - 288	${ m L}$	LCP
				7	288 - 304	U	RCP
				8	288 - 304	U	LCP
				9	304 - 320	${ m L}$	RCP
				10	304 - 320	${ m L}$	LCP
				11	320 - 336	U	RCP
				12	320 - 336	U	LCP
				13	336 - 352	${ m L}$	RCP
				14	336 - 352	${ m L}$	LCP
				15	352 - 368	U	RCP
				16	352 - 368	U	LCP
VERA4D*	1024	8	32	1	256 - 288	U	RCP
				2	256 - 288	U	LCP
				3	288 - 320	L	RCP
				4	288 - 320	L	LCP
				5	320 - 352	U	RCP
				6	320 - 352	U	LCP
				7	352 - 384	L	RCP
				8	352 - 384	L	LCP

^{*} GEO1D and VERA4D are also used for K/Q simultaneous mode. In this case, K-band is recorded in

digital filter unit (DFU) so that the amplitude losses at the edge of each baseband are avoided. This reduction is especially helpful to observe continuum sources, such as active galactic nuclei (AGN). For this purpose, C2 mode, which has 2 IFs \times 128 MHz, is opened for EAVN although the mode can be employed for an observation with only KaVA 7 telescopes.

When using the C2 mode, note the following two matters: (i) There is a moderate amplitude slope in an IF channel mainly at VERA stations, which must be corrected by all the gain calibration procedures in AIPS (AIPS tasks ACCOR, BPASS, and APCAL): (ii) KaVA's observation data is conventionally correlated by the Daejeon Hardware Correlator. In this case, the scaling factor of 1.3 should be applied to the data to recover the quantization loss ¹ [12].

^{*} the channels of odd number (RCP), while Q-band is recorded in the channels of even number (LCP).

 $[^]a$ Total number of channels

 $[^]b$ Bandwidth per channel in MHz

 $[^]c$ Channel number

^d Filtered frequency range in the base band (MHz)

^e Side Band (LSB/USB)

¹This scaling factor is conventionally applied to the data using the AIPS task APCAL, however this is not applicable if the data is loaded to AIPS using the AIPS task FITLD with DIGICOR = 3.

Table 8: Specification of The Daejeon correlator^a.

Max. number of antennas	16
correlation mode	$C2^b$ (128 MHz Bandwidth, 2 stream)
	C4 (32 MHz Bandwidth, 8 stream)
	C5 (16 MHz Bandwidth, 16 stream)
Max. number of corr./input	120 cross + 16 auto
Sub-array	2 case (12+4, 8+8)
Bandwidth	$512 \mathrm{\ MHz}$
Max. data rate/antenna	2048 Mbps VSI-H (32 parallels, 64 MHz clock)
Max. delay compensation	\pm 36,000 km
Max. fringe tracking	$1.075~\mathrm{kHz}$
FFT work length	16+16 bits fixed point for real, imaginary
Integration time	$25.6 \text{ msec} \sim 10.24 \text{ sec}$
Data output channels	8192 channels
Data output rate	Max. 1.4 GB/sec at 25.6 msec integration time

^aFor more details, see the following website: https://radio.kasi.re.kr/kjcc/main_kjcc.php

2.7 Calibration

Here we briefly summarize the calibration procedure of the EAVN data. Basically, most of the post-processing calibrations are done by using the AIPS (Astronomical Image Processing System) software package developed by NRAO (National Radio Astronomical Observatory).

2.7.1 Delay and Bandpass Calibration

The time synchronization for each antenna is kept within 0.1 μ sec using GPS and high stability frequency standard provided by the hydrogen maser. To correct for clock parameter offsets with better accuracy, bright continuum sources with accurately-known positions should be observed at usually every 60-80 minutes during observations. A recommended scan length for calibrators is 5-10 minutes. This can be done by the AIPS task FRING. The calibration of frequency characteristic (bandpass calibration) can be also done based on the observation of bright continuum source. This can be done by the AIPS task BPASS.

2.7.2 Gain Calibration

VERA, KVN, NRO45, TAK32, and HIT32 antennas have the chopper wheel of the hot load (black body at the room temperature), and the system noise temperature can be obtained by measuring the ratio of the sky power to the hot load power (so-called R-Sky method). Thus, the measured system noise temperature is a sum of the receiver noise temperature, spillover temperature, and contribution of the atmosphere (i.e. so-called T_{sys}^* corrected for atmospheric opacity). The hot load measurement can be made before/after any scan at all telescopes except TAK32 and HIT32. TAK32 and HIT32 measure the hot-load power at the timing when the telescope operator decides to do

^bThis mode is available for only KaVA.

the measurement before or after any scan. The sky power is continuously monitored during scans, so that one can trace the variation of the system noise temperature. The system noise temperature value can be converted to SEFD (System Equivalent Flux Density) by dividing by the antenna gain in K/Jy, which is derived from the aperture efficiency and diameter of each antenna. For the correlated data from KJCC, $T_{\rm sys}^*$ data (TY table) and antenna gain information (GC table) are provided with the ANTAB-readable format. KJCC makes complete version of ANTAB-readable file and provide it to PI. User support team supports PIs as appropriate. The TY and GC tables can be loaded by the AIPS task ANTAB, and these tables are converted to the SN table by the AIPS task APCAL.

On the other hand, T_{sys} measurement provided by TMRT65, SHRT25, and NSRT26 contains atmospheric opacity effects, thus the opacity correction should be applied to those data in the course of data reduction.

Alternatively, one can calibrate the visibility amplitude by the template spectrum method, in which auto-correlation spectra of a maser source is used as the flux calibrator. This calibration procedure is made by the AIPS task ACFIT (see AIPS HELP for ACFIT and [3] for more details). For an EAVN observation including TMRT65, NRO45, TAK32, HIT32, NSRT26, and SHRT25, we strongly recommend users to observe a maser source or a compact continuum gain calibrator for every ≤ 1 hr. This offers an additional cross-check of the amplitude calibration for TMRT65 and NRO45. YAM32 antenna is not equipped with any system noise temperature measurement system, and hence, it is mandatory to observe a maser source for the gain calibration and absolute flux scaling via the template spectrum method. KMRT40 antenna has a problem with the control program on the system of injecting noise source at each scan during observations, and hence, it is mandatory to observe a maser source for achieving the template spectrum method as well like the situation of YAM32. In particular during elevations lower than 20°, it is recommended to observe these calibrators every 30 min or shorter. Please see Section 3.10 for more details. The DPFU values used in the AIPS task ACFIT are listed in Table 4.

Further correction is made for VLBI observations taken with 2-bit (4-level) sampling, for the systematic effects of non-optimal setting of the quantizer voltage thresholds. This is done by the AIPS task ACCOR. Another correction should be applied to recover the amplitude loss, which are attributed to the combination of two steps of 2-bit quantization in the digital filtering at the backend system and characteristics of Daejeon correlator. This is done by multiplying the scaling factor of 1.3 (the best current estimation) [12] in the AIPS task APCAL (adverbs APARM(1) = 1.3, OPCODE = '', and DOFIT = 1) or SNCOR (adverbs OPCODE = 'MULA', and SNCORPRM(1) = 1.3). Note that this correction should be applied to all EAVN telescopes. The amplitude calibrations with EAVN are accurate to 15% or better at both K- and Q-bands.

For HIT32 at C-band, we recommend to flag the specified frequencies at the beginning of the data reduction: RF 6,600-6,648 MHz due to the IF filtering for anti-alias, and RF 6,712-6,760 MHz due to the Notch-filtering for flagging strong spurious. For example, after the digital filtering with GEO1S mode for HIT32 data, these frequencies correspond to IFs 1-3 and 8-10 in the correlated data in the C5 correlation mode (16 MHz \times 16 IFs). This flagging process is done by the AIPS task UVFLG.

2.7.3 Polarization Calibration

EAVN opens a dual-polarization mode at 22 and 43 GHz on a risk-shared basis. The data reduction procedures of polarimetric EAVN data are basically the same as those of other VLBI networks such as VLBA. For polarimetric VLBI data, there are three specific calibration steps, i.e., (1) calibration of the RCP-LCP delays, (2) calibration of polarization leakage terms (D-terms) and (3) absolute electric-vector-polarization angle (EVPA) corrections. For the RCP-LCP delay calibration (that can be performed using the AIPS task RLDLY), one must include a $\sim 2-3$ min scan of a very bright source (usually the source used for fringe-finder and bandpass is fine). For the Dterm calibration (that can be performed using the AIPS task LPCAL or GPCAL), one must insert a $\sim 5-10$ min scan of unpolarized or weakly-polarized sources every 1-2 hours covering a sufficient range of parallactic angles. Ideally the calibrators should be sufficiently compact, but moderately-resolved sources may also be used. For the EVPA calibration, one must include some scans of known EVPA sources. Absolute EVPA monitoring of compact radio sources at 22 or 43 GHz is regularly performed by some single-dish or connected-array facilities such as KVN single dish or VLA. For details, please consult with the support desk of these facilities through the EAVN user support team.

2.7.4 Pointing Correction

The EAVN two large telescopes, TMRT65 and NRO45, will carry out regular antenna pointing scans for every $\leq 1-2$ hr. As for TMRT65, moreover, frequent pointing check is necessary for observations at both K- and Q-bands. The pointing check is done semi-automatically with a continuum back-end system and the quality of pointing check is judged by on-site operators. We strongly recommend to keep at least 3 minutes for the pointing check itself with additional slewing time between target and pointing sources. For example, it is preferable to secure 5-min gap in total for the pointing check toward a pointing source with the angular separation of $\sim 15^{\circ}$ from the target.

2.8 Geodetic Measurement

2.8.1 Brief Summary of VERA Geodetic Measurement

Geodetic observations are performed as part of the VERA project observations to derive accurate antenna coordinates. The geodetic VLBI observations for VERA are carried out in the S/X-bands and also in the K-band. The S/X-bands are used in the domestic experiments with the Geographical Survey Institute of Japan and the international experiments called IVS-T2. On the other hand, the K-band is used in the VERA internal experiments. We obtain higher accuracy results in the K-band compared with the S/X-bands. The most up-to-date geodetic parameters are derived through geodetic analyses.

Non-linear post seismic movement of Mizusawa after the 2011 off the Pacific coast of Tohoku Earthquake continues. The position and velocity of Mizusawa is continuously monitored by GPS. The coordinates in Table 1 are provisional and will be revised with accumulation of geodetic data by GPS and VLBI.

In order to maintain the antenna position accuracy, the VERA project has three

kinds of geodetic observations. The first is participation in JADE (JApanese Dynamic Earth observation by VLBI) organized by GSI (Geographical Survey Institute) and IVS-T2 session in order to link the VERA coordinates to the ITRF2008 (International Terrestrial Reference Frame 2008). Basically Mizusawa station participates in JADE nearly every month. Based on the observations for four years, the three-dimensional positions and velocities of Mizusawa station till 2011 March 9 is determined with accuracies of 7 - 9 mm and about 1 mm/yr in ITRF2008 coordinate system. But the uncertainty of several centimeters exists in the position on and after 2011 March 11. The second kind of geodetic observations is monitoring of baseline vectors between VERA stations by internal geodetic VLBI observations. Geodetic positions of VERA antennas relative to Mizusawa antenna are measured from geodetic VLBI observations every two weeks. From polygonal fitting of the six-year geodetic results, the relative positions and velocities are obtained at the precisions of 1-2 mm and 0.8-1 mm/yrtill 2011 March 10. The third kind is continuous GPS observations at the VERA sites for interpolating VLBI geodetic positions. Daily positions can be determined from 24 hour GPS data. The GPS observations are also used to estimate tropospheric zenith delay of each VERA site routinely. The time resolution of delay estimates is 5 minutes.

2.8.2 Brief Summary of KVN Geodetic Measurement

KVN has been participating K band geodetic VLBI observations with VERA on behalf of KaVA geodesy program since 2011. In addition, the invariant point (IVP) coordinates of the KVN Ulsan and Tamna telescopes has been measured from the optical survey using GNSS and optical instruments. Please refer [22]. for more details. At present, the formal errors of KVN IVP in geodetic VLBI is around 3-5 mm and the difference between VLBI and GNSS is about 2 cm level.

3 Observing Proposal

3.1 Call for Proposals (CfP)

We invite proposals for the open-use observations of EAVN. Please refer to the following EAVN webpage for more details about the array and its performance, and how to prepare and submit a proposal.

This EAVN open-use call provides opportunities of VLBI observations at 6.7 GHz (C-band), 22 GHz (K-band), and 43 GHz (Q-band) for astronomers in the world. Nanshan 26-m telescope will be available at C-band from the 2024A semester on a shared-risk basis. If proposers are not familiar with EAVN, they are recommended to include at least one collaborator from EAVN. The contact address for the support is eavnhelp(at mark)kasi.re.kr.

EAVN observations have been conducted with single polarization (LCP²) until the 2022B semester, while the dual-polarization mode is also available in the shared-risk mode. The data are recorded with the data rate of 1 Gbps for both single- and dual-polarization mode. The data obtained at TAK32, HIT32, and YAM32 are recorded with the data rate of 2 Gbps and reformatted to 1 Gbps data at Mizusawa VLBI Observatory of NAOJ. The total observation time for EAVN is up to 416 hours, while the available observing time for each EAVN telescope is different between each other, as shown in Table 9.

Special conditions to be considered for EAVN proposal submission are shown below.

3.1.1 Total telescope time and maximum of total request time

Total telescope time to be provided by each telescope/array is as follows. Note that NRO45 and KMRT40 do not participate in the open-use program in the 2024A semester (Sections 2.2.3 and 2.2.10).

- Total telescope time for KaVA is 500 hours in 2024A while 84 hours are already allocated for one-year-long proposals approved in the 2023B semester. Thus, total 416 hours will be available for the proposals submitted in the 2024A semester. Proposers can request for the KaVA's telescope time (VERA+KVN) with no upper limit, while the maximum request time for non-KaVA telescopes per one proposal is 50 hours (24 hours for some telescopes). Refer to following items for a condition of the request time for each non-KaVA telescope. Note that a proposal for the Large Program will not be accepted for the 2024A semester. Note also that KaVA is a mandatory array for all EAVN observations.
- Sum of total telescope time for TMRT65 is 150 hours in 2024A while 35 hours are already allocated for one-year-long proposals approved in the 2023B semester. Thus, total 115 hours will be available for the proposals submitted in the 2024A semester. Proposers can request for the telescope time of up to 50 hours for TMRT65 for one proposal. Note that proposers cannot request for inclusion of both TMRT65 and SHRT25 in your project. SHRT25 will join EAVN C-band

²RCP is used for the simultaneous K/Q band mode (see Section 4.5).

Table 9: Available observing time and frequency for each EAVN telescope.

		Max. request			
Array/	Total	time for one		Frequency	r
Telescope	time [h]	proposal [h]	C-band	K-band	Q-band
KaVA	416		\bullet^1	•	•
Tianma (TMRT65)/	115^{2}	50	•	•	•
Sheshan (SHRT25)	_		•		
Nanshan (NSRT26)	150	50	•	•	
Takahagi (TAK32)	50	24		•	
Hitachi (HIT32)	50	24	$ullet^4$		
Yamaguchi (YAM32)	50	24	$ullet^4$		
Sejong (KSJ)	79^{5}	24		•	•

- 1: Five telescopes (VERA's 4 telescopes and KVN Ulsan) out of KaVA's 7 telescopes join EAVN observations at C-band.
- 2: Available time of the TMRT65 and SHRT25 antennas is 150h in total (not 150h for each).
- 3: Exactly total time and maximum time for one proposal is depends on its national missions, but negotiable.
- 4: HIT32 and YAM32 are simultaneously involved in EAVN open-use observations at C-band. Proposers shall not be able to choose only one of either HIT32 or YAM32 for their EAVN observations.
- 5: Sejong's telescope time is shared between EAVN open-use program (this call) and KVN open-use program.

observations in substitution of TMRT65 in case that TMRT65 cannot conduct EAVN observations.

- Total telescope time for NSRT26 is 150 hours. Proposers can request for the telescope time of up to 50 hours for NSRT26 for one proposal.
- Total telescope time for TAK32, HIT32, and YAM32 is 50 hours each. Proposers can request for the telescope time of up to 24 for each TAK32, HIT32, and YAM32 for one proposal.
- Total telescope time for KSJ is 100 hours in 2024A while 21 hours are already allocated for one-year-long proposals approved in the 2023B semester. Thus, total 79 hours will be available for the proposals submitted in the 2024A semester. Proposers can request for the telescope time of up to 24 hours for one proposal, while this telescope time is shared between EAVN open-use program (this call) and KVN open-use program. How to share KSJ's telescope time will be discussed between the Time Allocation Committee of EAVN and KVN on the basis of proposal review results. Note also that KSJ participates in EAVN open-use program in the 2024A semester with shared-risk mode for all observing modes to be provided.

3.1.2 Term of EAVN observation

- All EAVN observations will be scheduled between 2024 january 16 and 2024 June 15, while possible term of observation for each array/telescope is different between each other, as mentioned below.
- NRO 45-m, and Kunming 40-m telescopes will not be available in the 2024A semester due to the instrumental problems (Sections 2.2.3 and 2.2.10).

3.1.3 Possible array configuration

- KaVA is a mandatory array for all EAVN observations.
- At K- and Q-bands, EAVN accepts a request for usage of sub-array configuration (KaVA 7 telescopes and additional telescopes from TMRT65, NSRT26, TAK32, and KSJ for K-band and KaVA 7 telescopes and additional telescopes from TMRT65, and KSJ for Q-band) as well as EAVN full array configuration with 10 or 8 telescopes at K- or Q-band, respectively. A proposer shall clarify the reason for the choice of sub-array configuration in the proposal.
- HIT32 and YAM32 shall be simultaneously involved in EAVN open-use observations at C-band. Proposers shall not be able to choose only one of either HIT32 or YAM32 for their EAVN observations. Table 10 summarizes possible array configuration for EAVN observations at C-band.
- At C-band, either TMRT65 or SHRT25 will join the EAVN observations. When TMRT65 is not available, SHRT25 will be used in the EAVN observations.
- For the dual-polarization mode at K and Q bands, KJCC currently supports correlation of dual-polarization data up to 8 stations. In addition to KaVA 6 stations, one may request up to two additional station that supports dual-polarization reception. This may be TMRT65 (both K/Q bands), NSRT26 (only K band), and TAK32 (only K band).

In summary, non-KaVA telescopes (TMRT65/SHRT25, NSRT26, TAK32, HIT32, YAM32, and KSJ) will participate in EAVN observations together with KaVA according to scientific needs and their availability. Note that proposals submitted to EAVN can be assigned to KaVA according to the decision by the EAVN Time Allocation Committee (TAC).

Detailed information on the EAVN call-for-proposal can be found in the following webpage:

https://radio.kasi.re.kr/cfp.php?cate=EAVN

3.2 Proposal Submission

NOTE: In the 2024A semester, proposers are asked to submit a proposal via e-mail. Please see below for more details.

EAVN proposal submission deadline is at

Table 10: Possible array configuration at C-band.

-	10010 101	1 0001010 011	(a) 0011116a		301101.
Configuration			Tele	scope	
		TMRT65			
	$KaVA^a$	$\mathrm{SHRT}25^b$	NSRT26	$\mathrm{HIT}32^c$	$YAM32^c$
1	•				
2	•	0			
3	•		•		
4	•	0	•		
5	•			•	•
6	•	0		•	•
7	•		•	•	•
8	•	0	•	•	•

^a KaVA includes VERA 4 telescopes and KVN Ulsan (i.e. total 5 telescopes).

08:00 UT on 1 November, 2023.

The EAVN proposal application form and proposal information are available at the EAVN website:

EAVN proposal shall be submitted via e-mail to the following address.

Two PDF documents for a proposal cover sheet (two pages) and a body of proposal including scientific and technical justification including figures and tables (maximum of three pages; minimum font size of 11 points) should be attached on a message. Please send each proposal separately in case of submitting more than one proposal. Screening results for all submitted proposals will be announced to each PI by early January, 2024.

If you have any questions or requests regarding to your proposal, please contact also to eavnprop(at mark)kasi.re.kr.

3.3 Special Condition for Selecting Proposals

All submitted proposals for EAVN are reviewed by referees and the EAVN TAC allocates the observing time based on the referee's rating. A proposal submitted for EAVN observations could be allocated as KaVA observations depending on its rating and the decision made by TAC. Proposers thus should specify the necessity of including non-KaVA telescopes in your observations.

3.4 Policy of Recovery Observations

If an open use observation has more than one missing station due to system trouble and/or very severe weather conditions (e.g. strong wind due to a typhoon), the PI

^b Either TMRT65 or SHRT25 will join EAVN observations.

^c HIT32 and YAM32 shall be simultaneously involved in EAVN observations.

can request recovery observations within a year of receiving the correlated data. The EAVN TAC will consider the time allocation of the recovery observations for the next season. This policy is applied to EAVN telescopes except NRO45, KMRT40, and KSJ i.e., KVN, VERA, TMRT65/SHRT25, NSRT26, TAK32, HIT32 and YAM32.

3.5 Policy of One-year-long Proposals

EAVN accepts a proposal which requests observations across two successive semesters (2024A and 2024B semesters). Maximum of total request time for one proposal requesting for one-year-long observation shall be twice the telescope time for that requesting for half-year-long observation, i.e., 100 hours for TMRT65 and NSRT26, 72 hours for TAK32, HIT32, and YAM32, 48 hours for KSJ. No limitation on the total request time is set for KaVA. Proposers should clarify necessity of time allocation for two successive semesters in the proposal submitted. Note that EAVN TAC may allocate observing time within only one semester depending on the screening result.

3.6 Observation Mode

EAVN provides opportunities of observations at three observing frequencies, 6.7 GHz (C-band), 22 GHz (K-band), and 43 GHz (Q-band). By default, EAVN observations are conducted with single polarization (LCP³) and with the data recording rate of 1 Gbps (total bandwidth of 256 MHz). Up to 8 EAVN antennas including 7 KaVA stations can be used in the dual-polarization mode under the risk-share condition. Three types of setup of the digital filter ('C2 mode' with 2 IFs × 128 MHz, 'C4 mode' with 8 IFs × 32 MHz, and 'C5 mode' with 16 IFs × 16 MHz) are available, while the C2 mode is not available if your proposal contains requests for usage of non-KaVA stations. The C4 mode is available at all the frequencies, while the C5 mode can be used at both C- and K-bands. EAVN accepts a proposal using the 'Multi-frequency data recording mode' in which KVN records the observation data at more than one frequency, while total number of sessions using this mode might be limited depending on capability of disk storage. Note that multi-frequency mode and dual-polarization mode cannot be employed simultaneously for the EAVN session in the 2024A semester.

Available observing mode of EAVN is summarized in Tables 11 and 12.

3.7 Target of Opportunity (ToO) Observations

EAVN accepts ToO proposals. Proposers can request the participation of TMRT65, NSRT26, HIT32, TAK32, and YAM32 as well as KaVA for ToO observations, while these non-KaVA telescopes will join only on a best effort basis. Note that NRO45, KMRT40, and KSJ cannot be included for ToO proposals. Total approved time for ToO proposals is limited to be 100 hours in the 2024A semester.

It is strongly recommended that ToO proposals (especially expected ToO) are submitted during the regular CfP. Unexpected or urgent ToO can be submitted as Direc-

³RCP is used for the simultaneous K/Q band mode (see Section 4.5).

Table 11: Available observing mode of EAVN.

Frequency	C-band	K-band	Q-band			
Telescope	VERA, KVN-Ulsan,	KaVA, KSJ,	KaVA, KSJ,			
	TMRT65/SHRT25,	TMRT65, NSRT26,	TMRT65			
	NSRT26, HIT32, YAM32	TAK32	(9 telescopes)			
	(9 telescopes)	(11 telescopes)				
Backend mode	$C4, C5^a$	$C2^{b}, C4, C5$	$C2^b$, $C4$, $C5^c$			
Recording rate	1 Gbps^d					
Polarization	Left-hand circular polarization $(LCP)^e$					
	or Dual	circular polarization				
Correlator	Daejeon	Hardware Correlator				

^a For maser observations, C5 mode is strongly recommended to achieve sufficiently high channel resolution.

tor's Discretionary Time (DDT) proposals. ToO proposals must include clear triggering criteria to initiate an observation. ToOs are valid for one year after it is approved. ToO proposals for DDT should follow the same format of regular call and should be sent to eavnprop(at mark)kasi.re.kr.

3.8 Angular Resolution and Largest Detectable Angular Scale

The maximum angular resolution for EAVN observations is 1.8 mas at C-band for VERA-Ogasawara – NSRT26 baseline, 0.55 mas at K-band for VERA-Ogasawara – NSRT26 baseline, and 0.63 mas at Q-band for VERA-Mizusawa – VERA-Ishigakijima baseline in 2024A. Please revise by including Nanshan and/or excluding Kunming. The synthesized beam size strongly depends on UV coverage, and could be larger than the values mentioned above because the baselines projected on UV plane become shorter than the distance between telescopes. The beam size can be calculated approximately by the following formula;

$$\theta \sim 2063 \left(\frac{\lambda}{[\text{cm}]}\right) \left(\frac{B}{[\text{km}]}\right)^{-1} [\text{mas}],$$
 (4)

where λ and B are observed wavelength in centimeter and the maximum baseline length in kilometer, respectively.

The minimum detectable angular scale for interferometers can be also expressed by equation (4), where the baseline length B is replaced with the shortest one among the array.

Because of the relatively short baselines provided by KVN, ~ 300 km, KaVA is able to detect an extended structure up to 9 mas and 5 mas for the K- and Q-bands, respectively. As for an EAVN array in which non-KaVA stations (except NSRT26 and

^b C2 mode is available at only KaVA telescopes.

^c C5 mode is available at KaVA and TMRT65.

^d Data obtained at TAK32, HIT32, and YAM32 are recorded with 2 Gbps and reprocessed to 1 Gbps.

 $^{^{}e}$ RCP is used for the simultaneous K/Q band mode (see Section 4.5).

Table 12: Available observing mode for each EAVN telescope.

		Band	l			(Observin	g mode		
Telescope	\overline{C}	K	Q	$\overline{\mathrm{T.I.}^a}$	$F.S.^b$	HB^c	WFI^d	$K/Q^{e,f}$	$2\text{-pol}^{f,g}$	ToO^h
KaVA	$ullet^i$	•	•	•	•	•	•	•	•	•
TMRT65	•	•	•	•					•	•
SHRT25	•			•						
NSRT26	•	•		•	•				●(K)	•
TAK32		•		•					•(K)	•
HIT32	•			•	•					•
YAM32	•			•	•					•
KSJ		•	•	•	•			•		

^a Total intensity imaging.

KMRT40) are added to KaVA, the shortest baseline became 120 km between KYS and KSJ. Thus the largest detectable angular scales will be improved by a factor of ~ 2.5 in K- and Q-band. In the case of C-band where KSJ does not participate, the first, second, and third shortest baseline formed by KVN-Ulsan – YAM32, VERA-Mizusawa – HIT32 and VERA-Iriki – YAM32 is similar to be ~ 260 km, ~ 270 km and ~ 290 km, yielding 36, 34 and 32 mas in C-band, respectively.

Because the longest baselines remain unchanged, the maximum angular resolutions are basically the same as those of KaVA, although their detailed values in a synthesized image are dependent on the scheme of UV weighting as well as the UV coverage. As for an EAVN array which additionally includes NSRT26 for both at C-band and K-band, the longest baseline length extends to 5100 km (primarily along the east-west direction). This enhances the maximum angular resolution at C-band and K-band of EAVN by a factor of ~ 3 compared to that of KaVA from 2024A and 2021B, respectively.

3.9 Sensitivity

When a target source is observed, a noise level $\sigma_{\rm bl}$ for each baseline in the single-polarization can be expressed as

$$\sigma_{\rm bl} = \frac{2k}{\eta} \frac{\sqrt{T_{\rm sys,1} T_{\rm sys,2}}}{\sqrt{A_{\rm e,1} A_{\rm e,2}} \sqrt{2B\tau}} = \frac{1}{\eta} \frac{\sqrt{SEFD_1 SEFD_2}}{\sqrt{2B\tau}},\tag{5}$$

where k is Boltzmann constant, η is quantization efficiency (~ 0.88), $T_{\rm sys}$ is system noise temperature, SEFD is system equivalent flux density, A_e is antenna effective aperture area ($A_e = \pi \eta_A D^2/4$ in which η_A and D are the aperture efficiency and antenna diameter, respectively), B is the bandwidth, and τ is on-source integration time. Note that for an integration time beyond 3 minutes (in the K-band), the noise level expected by equation (5) cannot be attained because of the coherence loss due

^b Fast antenna switching. See Section 4.2.

^c 1-beam hybrid mode. See Section 4.3.

^d Wide-field imaging with short accumulation period. See Section 4.4.

 $^{^{}e}$ K/Q-band simultaneous observation mode. See Section 4.5.

 $[^]f$ K/Q-band multi-frequency mode and dual-polarization mode cannot be employed simultaneously for the EAVN session in the 2024A semester.

 $[^]g$ Dual circular polarization at K- and Q-bands. See Section 4.1

^h Target of opportunity. See Section 3.7.

ⁱ VERA four stations and KVN Ulsan station.

to the atmospheric fluctuation. Thus, for finding fringe within a coherence time, the integration time τ cannot be longer than 3 minutes. For VLBI observations, signal-to-noise ratio (S/N) of at least 5 and usually 7 is generally required for finding fringes.

A resultant image noise level $\sigma_{\rm im}$ can be expressed as

$$\sigma_{\rm im} = \frac{1}{\sqrt{\Sigma \sigma_{\rm bl}^{-2}}}.$$
 (6)

If the array consists of identical antennas, an image noise levels can be expressed as

$$\sigma_{\rm im} = \frac{2k}{\eta} \frac{T_{\rm sys}}{A_e \sqrt{N(N-1)B\tau}} = \frac{1}{\eta} \frac{SEFD}{\sqrt{N(N-1)B\tau}},\tag{7}$$

where N is the number of antennas. Using the typical parameters shown in Tables 13-15, baseline and image sensitivity values in the single-polarization of EAVN can be calculated as listed in Tables 13-15 and Tables 16-17, respectively (baseline and image sensitivities of KVN, VERA, and KaVA, as well as EAVN, are also shown for reference). Tables 13-15 contains all combinations of baselines, while Tables 16-17 indicates part of possible combinations of telescopes.

Figures 21 and 22 show the system noise temperature at VERA and KVN-Ulsan in K/Q-bands, and VERA-Ogasawara in C-band, respectively. VERA, receiver noise temperatures are also plotted.

Note that the receiver temperature of VERA includes the temperature increase due to the feedome loss and the spill-over effect. In Mizusawa, typical system temperature in the K-band is $T_{\rm sys}=150~{\rm K}$ in fine weather of winter season, but sometimes rises above $T_{\rm sys}=300~{\rm K}$ in summer season. The system temperature at Iriki station shows a similar tendency to that in Mizusawa. In Ogasawara and Ishigakijima, typical system temperature is similar to that for summer in Mizusawa site, with typical optical depth of $\tau_0=0.2\sim0.3$. The typical system temperature in the Q-band in Mizusawa is $T_{\rm sys}=250~{\rm K}$ in fine weather of winter season, and $T_{\rm sys}=300-400~{\rm K}$ in summer season. The typical system temperature in Ogasawara and Ishigakijima in the Q-band is larger than that in Mizusawa also.

On the other hand, system noise temperature in C-band is stable around 100–150 K at all the VERA stations through all the season with typical zenith optical depth of $\tau_0 = 0.03 \sim 0.04$, although it sometimes show larger values due to extremely bad weather condition.

The typical system temperature in the K-band at all KVN stations is around 100 K in winter season. In summer season, it increases up to ~ 300 K. In the Q-band, the typical system temperature is around 150 K in winter season and 250 K in summer season at Yonsei and Tamna. The system temperature of Ulsan in the Q-band is about 40 K lower than the other two KVN stations. This is mainly due to the difference in receiver noise temperature (see Table 5).

In the dual-polarization mode, the baseline sensitivity to each polarization will be degraded by a factor of $\sqrt{1/2}$ since the total recording rate is fixed to 1 Gbps and the bandwidth for each polarization becomes a half of that in the single polarization mode.

_	•
. C	2
_	
ά.	3
~	۲
_	4
Ų	_
\simeq	
_	
+	٥
Ċ	3
•	_
-	-
Z	4
\	>
	4
◁	4
r-	١
\vdash	
٠.	
$\overline{}$	
_	-
а	ì
~	5
_ >	4
-	
α	3
- 5-	÷
٤	
)
÷	+
- 5	
4	,
Д	
	ľ
\mathcal{C}	
_	4
а	b
_	
$\overline{}$	2
΄ α	₹
⊏,	5

		TADIC TO	O. 1 CITO	HIGHEO .	Table 19: I citofilialice of Livin at IN-Dalid.	to IX-Dail			
Ante	nna per	Antenna performance			Basel	Baseline sensitivity	vity		
$T_{\rm sys}$	η_{A}	SEFD	KVN	VERA	TMRT65	NRO45	NSRT26	TAK32	KSJ
X		[Jy]							
100	9.0	1328	6.1	7.7	1.7	2.8	3.2	3.1	5.9
120	0.5	2110	I	9.7	2.1	3.6	4.0	3.9	7.4
09	0.5	100	I	I	I	8.0	6.0	8.0	1.6
100	0.61	285	I	I	I	I	1.5	1.4	2.7
42	9.0	364	I	I	I	I	I	1.6	3.1
40	0.3	343	I	I	I	I	I	I	3.0
100	0.59	1231	I	I	I	Ι	I	Ι	I

assume an integration time of 120 seconds and a bandwidth of 256 MHz for the calculation. In the Note: The 1σ baseline sensitivity values for the single-polarization are listed in unit of mJy, which case of narrower bandwidth of 15.625 kHz (for maser emission), sensitivities can be calculated by multiplying a factor of 128.

Table 14: Performance of EAVN at Q-band.

	'		110110 1 11	TO COTTONIA	1 1 1 1	table to the interior of the track of the track		
	Ante	nna per	Antenna performance		B	Baseline sensitivity	ivity	
	$T_{\rm sys}$ $[{ m K}]$	η_{A}	$\frac{\text{SEFD}}{[\text{Jy}]}$	KVN	VERA	KVN VERA TMRT65 NRO45	NRO45	KSJ
	150	9.0		9.1	13.6	2.3	5.2	9.3
VERA	250	250 0.5		I	20.1	3.4	7.8	13.8
$_{ m TMRT65}$	99	0.45		I	I	I	1.3	2.3
NRO45	200	0.53		I	I	I	I	5.3
KSJ	150	0.53		I	I	I	I	

Note: The 1σ baseline sensitivity values for the single-polarization are listed in unit of mJy, which assume an integration time of 120 seconds and a bandwidth of 256 MHz for the calculation. In the case of narrower bandwidth of 15.625 kHz (for maser emission), sensitivities can be calculated by multiplying a factor of 128.

Table 15: Performance of EAVN at C-band.

	Ante	intenna performan	formance			Base	Baseline sensitivi	vity		
	$T_{ m sys}$	η_{A}	SEFD	VERA	TMRT65	SHRT25	NSRT26	KMRT40	HIT32	YAM32
	Ξ		[Jy]							
KVN Ulsan	330	0.62	4241	13.9	2.2	12.5	7.1	5.2	3.8	5.0
VERA	130	0.53	2155	6.6	1.6	8.9	5.1	3.7	2.7	3.6
$ ext{TMRT}65$	30	0.45	55	I	I	I	8.0	0.0	0.4	9.0
SHRT25	130	0.42	1740	I	I	I	4.6	3.4	2.4	3.2
NSRT26	55	0.50	572	1	I	I	I	1.9	1.4	1.9
KMRT40	35	0.25	307	I	I	I	I	I	1.0	1.4
HIT32	30	0.65	158	I	I	I	I	I	I	1.0
YAM32	20	0.60	286	I	I	I	I	I	I	I
	,									

Note: The 1σ baseline sensitivity values for the single-polarization are listed in unit of mJy, which assume an integration time of 120 seconds and a bandwidth of 256 MHz for the calculation. In the case of narrower bandwidth of 1.953 kHz (for maser emission), sensitivities can be calculated by multiplying a factor of 362.

Table 16: Image sensitivity of EAVN at K- and Q-bands.

Array	$N_{\rm ant}$	$N_{\rm bl}$	K-band	Q-band
KVN	3	3	320	480
VERA	4	6	360	750
KaVA	7	21	219	379
KaVA+TMRT65	8	28	85	125
KaVA+NRO45	8	28	126	239
KaVA+TMRT65+NRO45	9	36	60	95
KaVA+TMRT65+NSRT26	9	36	63	_
KaVA+TMRT65+KSJ	9	36	76	113
KaVA+NRO45+KSJ	9	36	111	209
KaVA+TMRT65+NSRT26+NRO45	10	45	49	_
KaVA+TMRT65+NRO45+KSJ	10	45	56	89
KaVA+TMRT65+NSRT26+KSJ	10	45	59	_
KaVA+TMRT65+NSRT26+NRO45+TAK32	11	55	41	_
KaVA+TMRT65+NSRT26+NRO45+KSJ	11	55	46	_
KaVA+TMRT65+NSRT26+NRO45+TAK32+KSJ	12	66	39	_

Note: $N_{\rm ant}$ and $N_{\rm bl}$ are the numbers of telescopes and baselines for each array, respectively. The 1σ image sensitivity values in the single-polarization mode are listed in unit of μ Jy, which assume an integration time of 4 hours and a total bandwidth of 256 MHz for the calculation. In the case of narrower bandwidth of 15.625 kHz (for maser emission in K/Q-bands) and 1.953 kHz (for maser emission in C-band), sensitivities can be calculated by multiplying a factor of 128 and 362, respectively.

3.10 Calibrator Information

The NRAO VLBA calibrator survey is very useful to search for a continuum source which can be used as a reference source to carry out the delay, bandpass, and phase calibrations. The source list of this calibrator survey can be found at the following VLBA homepage:

http://www.vlba.nrao.edu/astro/calib/index.shtml https://obs.vlba.nrao.edu/cst/

For delay calibrations and bandpass calibrations, calibrators with 1 Jy or brighter are strongly recommended as listed in the VLBA fringe finder survey:

http://www.vlba.nrao.edu/astro/fringe_finder_survey/ffs.html https://science.nrao.edu/facilities/vlba/publications/memos/test/ffs

Interval of observing calibrator scans must be shorter than 1 hour to track the delay and delay rate in the correlation process.

If you request the participation of the YAM32 and/or KMRT40 and/or NSRT26 antennas for observations in C-band, it is mandatory to do gain calibration and absolute flux scaling by the template spectrum method. In this method, a strong and compact CH₃OH maser source which locates within 15° from the target source should be observed with an interval of 1 hr or shorter. In particular during elevations lower than 20°, it is recommended to observe these calibrators every 30 min or shorter. Even

Table 17: Image sensitivity of EAVN at C-band.

Array	$N_{ m ant}$	$N_{\rm bl}$	C-band
KaVA+TMRT65	6	15	94
KaVA+SHRT25	6	15	346
KaVA+KMRT40	6	15	203
KaVA+NSRT26	6	15	255
KaVA+HIT32+YAM32	7	21	89
KaVA+TMRT65+KMRT40	7	21	58
KaVA+SHRT25+KMRT40	7	21	174
KaVA+TMRT65+NSRT26	7	21	68
KaVA+SHRT25+NSRT26	7	21	215
KaVA+TMRT65+HIT32+YAM32	8	28	37
KaVA+SHRT25+HIT32+YAM32	8	28	83
KaVA+HIT32+YAM32+KMRT40	8	28	65
KaVA+HIT32+YAM32+NSRT26	8	28	73
KaVA+TMRT65+HIT32+YAM32+KMRT40	9	36	31
KaVA+SHRT25+HIT32+YAM32+KMRT40	9	36	62
KaVA+TMRT65+HIT32+YAM32+NSRT26	9	36	34
KaVA+SHRT25+HIT32+YAM32+NSRT26	9	36	69
KaVA + TMRT65 + HIT32 + YAM32 + KMRT40 + NSRT26	10	45	29
KaVA+SHRT25+HIT32+YAM32+KMRT40+NSRT26	10	45	54

Note: $N_{\rm ant}$ and $N_{\rm bl}$ are the numbers of telescopes and baselines for each array, respectively. The 1σ image sensitivity values in the single-polarization mode are listed in unit of μ Jy, which assume an integration time of 4 hours and a total bandwidth of 256 MHz for the calculation. In the case of narrower bandwidth of 15.625 kHz (for maser emission in K/Q-bands) and 1.953 kHz (for maser emission in C-band), sensitivities can be calculated by multiplying a factor of 128 and 362, respectively.

if YAM32 and/or KMRT40 and/or NSRT26 antennas are not included in the observations, it is recommended to observe the strong and compact CH₃OH maser source with the same interval as the cross-check for the gain curve and absolute flux scaling of the TMRT65 antenna as well. The 6.7 GHz CH₃OH maser sources close to your target sources can be found in the following catalog papers (NOTE: in the template spectrum method for the TMRT65 in C-band, it is NOT recommended that the 6.7 GHz CH₃OH maser sources 009.621+0.196, 133.94+1.04 (W3(OH) / W3-IRS5), and 351.417+0.645 & 351.417+0.646 (NGC6334F) are selected because these sources are too strong for the TMRT65 to guarantee an accuracy of the absolute flux scaling.):

Methanol MultiBeam (MMB) Survey:

```
20^{\circ} \leq l \leq 60^{\circ}: \ \text{https://academic.oup.com/mnras/article/450/4/4109/1747594} \\ 6^{\circ} \leq l \leq 20^{\circ}: \ \text{https://academic.oup.com/mnras/article/409/3/913/1094145} \\ 345^{\circ} \leq l \leq 6^{\circ}: \ \text{https://academic.oup.com/mnras/article/404/2/1029/968927} \\ 330^{\circ} \leq l \leq 345^{\circ}: \ \text{https://academic.oup.com/mnras/article/417/3/1964/1090874} \\ 186^{\circ} \leq l \leq 330^{\circ}: \ \text{https://academic.oup.com/mnras/article/420/4/3108/972699} \\ \label{eq:definition}
```

Ibaraki 6.7 GHz class II methanol maser database (iMet):

http://vlbi.sci.ibaraki.ac.jp/iMet/

Other catalog for sources in more northern hemisphere:

https://www.aanda.org/articles/aa/abs/2009/44/aa12135-09/aa12135-09.html

For dual-polarization analysis, one should include calibrators for (1) calibration of the RCP-LCP delays, (2) calibration of polarization leakage terms (D-terms) and (3) EVPA corrections. See also Section 2.7.3 for more detail.

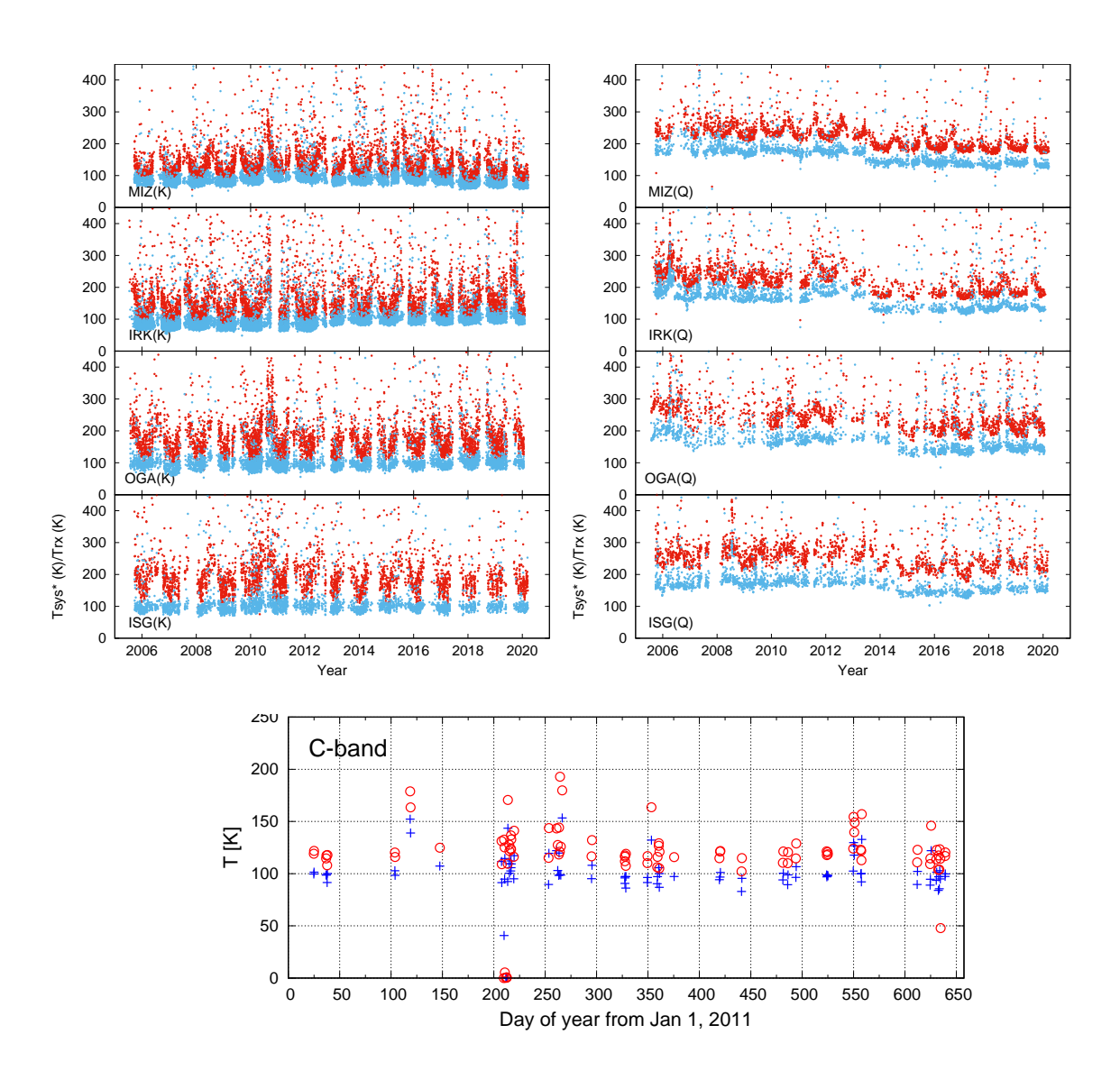


Figure 21: The receiver noise temperature (*blue*) and the system noise temperature (*red*) at the zenith for the VERA antennas at K-band (top-left), Q-band (top-right), and at C-band in Ogasawara station (bottom).

3.11 Data Archive

The users who proposed the observations will have an exclusive access the data for 18 months after the correlation. After that period, all data for EAVN open-use observations will be released as archive data. Thereafter, archived data will be available to any user upon request. This policy is applied to each observation, even if the proposed observation is comprised of multi-epoch observations in this season.

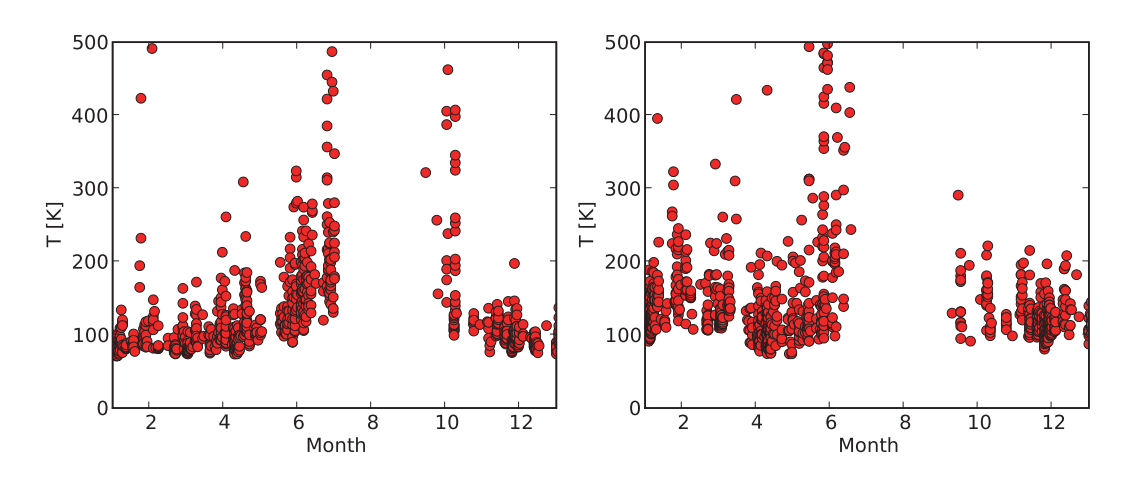


Figure 22: The zenith system noise temperature (red filled circles) at K-band (left) and Q-band (right) in KVN-Ulsan station.

4 Notes for Special Modes

In this section, we summarize additional information about special observing/data analysis modes.

4.1 Dual Circular Polarization

The dual-circular-polarization mode is available at the K- and Q-band from the EAVN open use 2024A on a risk-shared basis. The EAVN performance evaluation team (PET) is now verifying polarimetry observation data by comparing the newly correlated data from KJCC and DiFX. Note that multi-frequency mode and dual-polarization mode cannot be employed simultaneously for the EAVN session in the 2024A semester. Further details will be available upon request through the EAVN user support team.

4.2 Phase-referencing and Astrometry

EAVN is capable of phase-referencing observations to image weak target sources, which cannot be detected within coherent time, and to conduct absolute astrometry measurements. Note that astrometry capability has been confirmed for K-band observations with KaVA 7 telescopes. Although we do not prevent EAVN proposers from submitting proposals with the phase-referencing mode at Q-band and/or with the mode using non-KaVA telescopes within the maximum driving speed of each antenna shown in Table 3, the data quality is not guaranteed. From the semester 2021A, we opened the fast-switching (not astrometry mode) mode in C-band as well. In 2024A, the following antenna combination among KaVA+HIT32+YAM32 is available (see the notification in sub-section 4.2.1).

4.2.1 Fast Switching

Fast switching observation with EAVN is recommended for phase referencing (and astrometry) since the verification of the fast switching with EAVN has been finished, except for TMRT65, NRO45 and TAK32 telescopes. In this mode, the antenna nods between phase calibrator (reference) and target source. With this mode, we can detect and image weak sources, which can not be imaged directly by fringe fitting. Regarding antenna switching cycle, users can refer to Table 18.

4.2.2 Notification for Switching Cycle in C-band

In the fast-switching in C-band, we recommend typical time of each switching cycle of 5–6 min, which was observationally verified successful phase-referencing imaging without serious issues and a few milliarcsecond accuracies of absolute position measurements. When you decide the switching cycle, it is necessary to take into account the slewing time of HIT32 that has the slowest driving speed of 0.2° sec⁻¹. We thus present a simulated result of antenna slewing time of HIT32. Figure 23 plots the relationship between the slewing time in one way between target and reference continuum sources as a function of elevation angles for the target–calibrator separation angles

\mathbf{m} 11	10	Di .	D (•	α 1	m·	/ · '	\ *
Table	$1 \times \cdot$	Phase-	Referen	าคากต	CACLE	Times	min	1
Table	10.	I Hase .		CHI	\circ	1111100	TITITI	, .

	Tymic	al wasther	Dad	rrroothon	Cood	weather
	V 1	cal weather		weather		
	($2 \times 10^7 \text{ m}^{-1/3}$	($4 \times 10^7 \text{ m}^{-1/3}$,	$\times 10^7 \text{ m}^{-1/3})$
	Freque	ency (GHz)	Freque	ency (GHz)	Freque	ncy (GHz)
EL (deg)	22	$(43)^{\ddagger}$	22	$(43)^{\ddagger}$	22	$(43)^{\ddagger}$
5	0.3	0.2	0.2	0.1	0.8	0.4
10	0.5	0.3	0.2	0.1	0.8	0.6
15	0.7	0.3	0.3	0.1	1.5	0.7
20	0.8	0.4	0.3	0.2	1.8	0.9
25	0.9	0.4	0.4	0.2	2.0	1.0
30	1.0	0.5	0.4	0.2	2.8	1.1
40	1.1	0.5	0.5	0.2	5.8	1.3
50	1.3	0.6	0.6	0.3	9.9	1.5
60	1.8	0.7	0.6	0.3	10.0	2.2
70	2.3	0.7	0.6	0.3	10.0	2.9
80	2.6	0.7	0.6	0.3	10.0	3.3

^{*} Referring to Ulvestad, J., Phase-Referencing Cycle Times, VLBA Scientific Memo 20 (1999).

Column 1 shows antenna elevation angles. Columns 2-3 indicate phase-referencing cycles at 22 and 43 GHz, respectively, under typical weather condition. The phase-referencing cycle is defined as the time between the midpoints of the two calibrator observations before and after the target observation. Columns 4-5 are the same as Columns 2-3, but with bad weather condition (similar to some summer days). Columns 6-7 are the same as Columns 2-3, but with good weather condition (similar to some winter nights).

(S.A.) of 1 and 2 deg. From Figure 23, it is strongly recommended to schedule the fast-switching observations with elevation angles lower than 80 and 70 deg in the case of S.A. of 1 and 2 deg, respectively. Finally, proposers are required to specify each on-source time for target and reference continuum sources in one switching cycle at C-band in scientific or technical justification in the proposal.

4.2.3 Separation Angle between Target and Phase Reference

It is strongly recommended to observe a pair sources with a small separation angle (e.g., less than 1 degree) at high elevation for precise astrometry. For instance, it is demonstrated that the dynamic range of the phase-referenced image is inversely proportional to the sine of the calibrator-to-target separation as

$$D_1 = \left(\frac{\sqrt{\Delta t}}{K\nu}\right) \left(\sin\theta_{\text{sep}}\right)^{-1},\tag{8}$$

where Δt is the on-source observing time, ν , the observing frequency, θ_{sep} , the separation angle between the target and calibrator, and K, a constant to be determined [13].

4.2.4 Tropospheric Calibration with GPS or JMA or Geodetic Blocks

Generally, residual of atmospheric zenith delay dominates cm-wave VLBI positional accuracy. Atmospheric (tropospheric) calibration for EAVN has three options (see Table 19), which are (1) GPS, (2) Japan Meteorological Agency (JMA) meso-scale

^{\dagger} C_n is strength of the tropospheric turbulence.

[‡] Currently, Q-band phase-referencing mode is under evaluation.

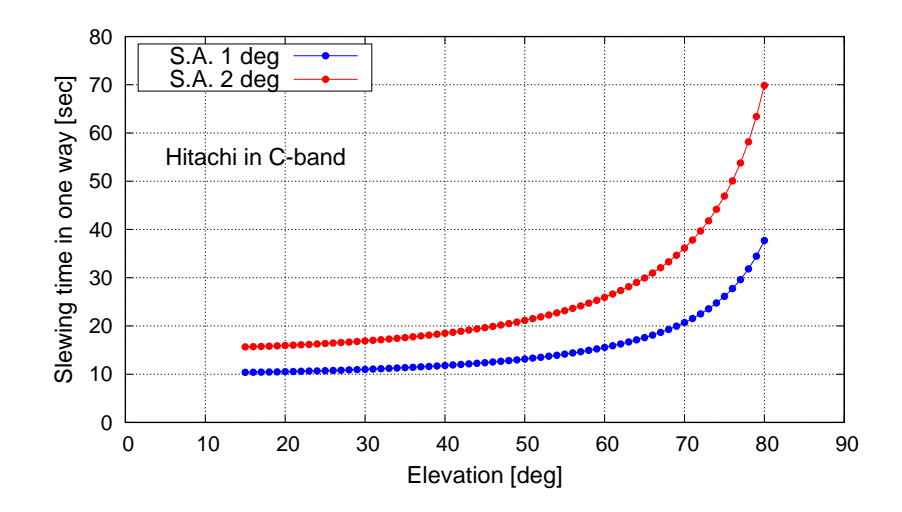


Figure 23: Simulated result of antenna slewing time of HIT32 at C-band in one way between target and reference continuum sources. This simulation shows a dependence on elevation, and a difference in the case of the separation angle of 1 deg (blue filled circles) and 2 deg (red filled circles).

analysis data (Hobiger et al. 2008; JMA Numerical Weather Prediction¹), and (3) Geodetic blocks². An error of tropospheric zenith delay ($c\Delta\tau_{\text{trop}}$) can be suppressed within \sim 2 cm with GPS, JMA and Geodetic blocks [9, 14].

Table 19: Tropospheric calibration for each EAVN telescope*.

Telescope		Method				
	GPS	JMA	Geodetic blocks			
VERA	•	•	•			
KVN	\triangle	•	•			
TMRT65	\triangle	•	•			
NSRT26	\triangle	×	•			

^{*} TMRT65 = Tianma 65m. NSRT26 = Nanshan 26m. \bullet = Available. \triangle = These GPS receivers should be evaluated for the usage of astronomical (i.e., astrometry) purpose. \times = Not available.

4.2.5 Astrometric Accuracy

We have verified astrometric accuracies of KaVA and EAVN based on (1) a Galactic line source and (2) QSO pair observations (see Figures 24 and 25, and Tables 20 and 21). Single-epoch (relative) astrometric error consists of (1) thermal and (2) systematic errors as shown below [19]:

$$\Delta \theta_{\text{therm}} \approx 31 \left(\frac{22}{\nu \text{ [GHz]}} \right) \left(\frac{2,300}{B_{\text{max}} \text{ [km]}} \right) \left(\frac{20}{\text{S/N}} \right) [\mu \text{as}]$$
 (9)

and

¹https://www.jma.go.jp/jma/jma-eng/jma-center/nwp/nwp-top.htm

²http://bessel.vlbi-astrometry.org/tech

$$\Delta s_{\rm rel} \approx 31 \left(\frac{{\rm c}\Delta \tau \ [{\rm cm}]}{2}\right) \left(\frac{2,300}{B_{\rm max}\ [{\rm km}]}\right) \left(\frac{\theta_{\rm sep}\ [{\rm deg}]}{1}\right) [\mu {\rm as}]$$
 (10)

where ν is the observing frequency, B_{max} , the longest baseline length, S/N, signal-to-noise ratio of a phase-referenced image, $c\Delta\tau$, the speed of light multiplied by delay residual, and θ_{sep} , separation angle between the target and a calibrator (a phase reference).

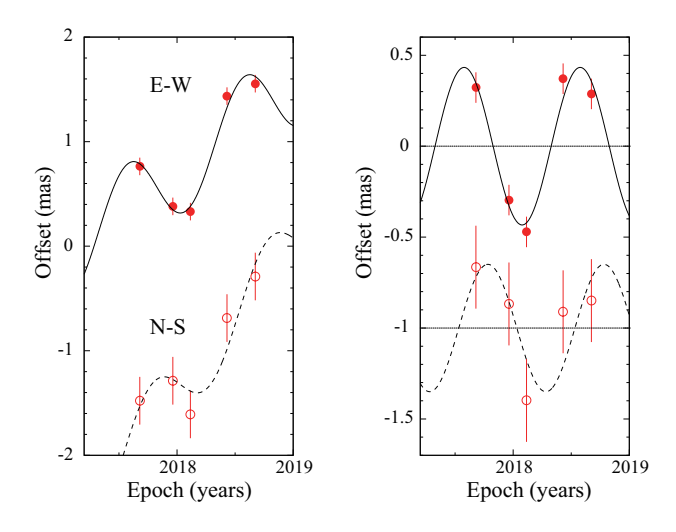


Figure 24: Results of parallax and proper-motion fitting. Plotted are position offset of maser spot (W3(OH) at $V_{\rm LSR} = -47.5~{\rm km~s^{-1}}$) with respect to the background QSO J0244+6228 (with a separation angle of 2.2 degrees) toward the east (R.A.cos σ) and north (σ) as a function of time. For clarity, the north direction data is plotted offset from the east direction data. (*Left*) The best-fit models in the east and north directions are shown as continuous and dashed curves, respectively. (*Right*) Same as the Left, but with proper motions removed.

Table 20: Parallax results for W3(OH)*.

Array	Frequency	Source	$V_{ m LSR}$	Parallax	$\sigma_{lpha \cos \delta}^*$	σ_{δ}^*	Ref.
	GHz		${\rm km~s^{-1}}$	(mas)	(mas)	(mas)	
KaVA	22	W3OH	-47.5	$0.460 {\pm} 0.035$	0.052	0.256	
VLBA	22	W3OH	$-51.5 \sim -48.2$	$0.489 {\pm} 0.017$	$\sim \! 0.050$	~ 0.050	(1)

^{*}Positional errors in right ascension and declination were adjusted so that the reduced chi-square becomes unity. Columns 1-2 represent array and observing frequency. Columns 3-4 show source name and LSR velocity of the maser spot, used for the parallax fit. Column 5 displays the parallax result in milli-arcseconds (mas). Columns 6-7 represent the (systematic) positional errors in right ascension and declination, respectively.

Ref. (1) Hachisuka et al. (2006).

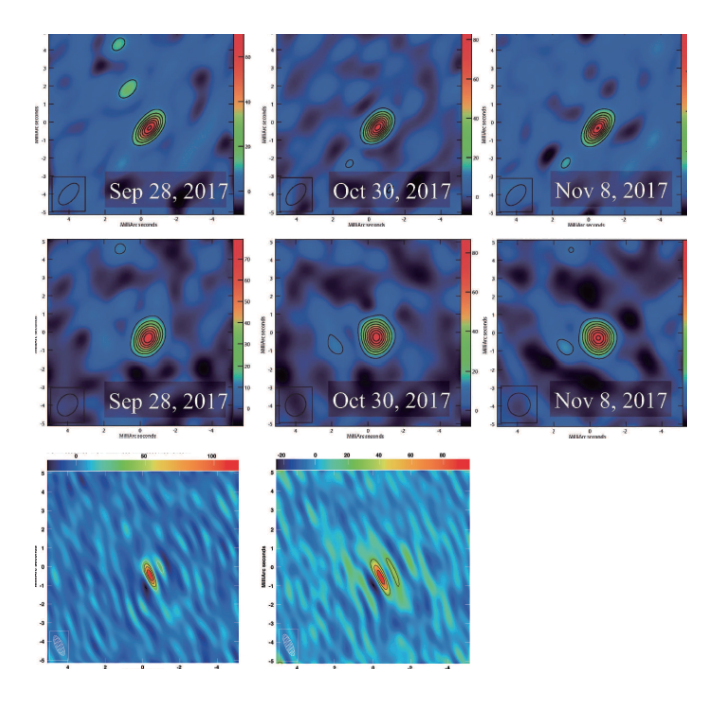


Figure 25: (**Top row**) Phase-referenced images of 0556+238 with VERA, relative to the phase reference 0601+245. The dates of the observations are Sep 28, Oct 30 and Nov 8 in 2017 from left to right. (**Middle row**) Same as the top row, but for KaVA data used. (**Bottom row**) Same as the top row, but for EAVN data used. Observation dates are Mar 27 and May 24 in 2019 from left to right.

Table 21: Results of position repeatability for 0556+238.

Table 21. Resides of position repositioning for 6550 (256)						
	VE	ERA	Ka	VA	EA	VN
Observation date	R.A.	Decl.	R.A.	Decl.	R.A.	Decl.
	(μas)	(μas)	(μas)	(μas)	(μas)	(μas)
$2017/{\rm Sep}/28$	-465 ± 15	-332 ± 16	-451 ± 15	-331 ± 15	_	_
2017 Oct / 30	-494 ± 11	-283 ± 12	-462 ± 16	-258 ± 18	_	_
2017/Nov/8	-505 ± 09	-318 ± 10	-480 ± 13	-287 ± 14	_	_
$2019/\mathrm{Mar}/27$	-463 ± 21	-343 ± 24	-464 ± 14	-336 ± 17	-407 ± 11	-455 ± 21
2019/May/24	-576 ± 85	-479 ± 150	-592 ± 29	-434 ± 35	-411 ± 24	-524 ± 44
Unweighted mean	-500 ± 21	-351 ± 34	-490 ± 26	-330 ± 30	-409 ± 2	-490 ± 35

Column 1 shows the date of observation. Columns 2-3 display image positions of 0556+238 relative to 0601+245 in right ascension and declination, respectively. Note that the image positions were measured for VERA data. The errors of the positions represent the thermal error. Columns 4-5 are the same as the Columns 2-3, but for KaVA data used. Columns 6-7 are the same as the Columns 2-3, but for EAVN data used.

YAM32KUS KTN TM65 NS26 SH25 HIT32 Table 22: Baseline lengths for EAVN astrometry.* ISG KYS IRK

MIZ

KM40

												2,900	-
											006	3,800	1
										1,900	1,000	1,900	1
									3,300	4,500	3,900	2,500	3,400
								3,300	ı	1,900	1,000	1,900	800
							009	3,600	I	I	I	I	400
						400	006	3,700	006	1,000	300	2,800	200
					300	200	006	3,400	I	I	I	I	100
				1,800	1,300	1,000	800	4,000	800	2,100	1,300	2,200	1,400
			1,800	1,800	1,500	1,700	2,100	5,200	2,100	1,100	1,300	3,900	1,800
		1,300	1,000	200	400	400	006	4,000	006	1,100	300	2,800	009
	1,300	1,300	2,300	1,200	1,100	1,500	2,000	4,500	2,000	300	1,000	3,900	1,300
MIZ	IRK	OGA	ISG	KYS	KUS	KTN	TM65	NS26	SH25	HIT32	YAM32	KM40	KSJ

* The unit is (km). Each value is rounded off to the (nearest) 100. MIZ=VERA-

Mizusawa; IRK=VERA-Iriki; OGA=VERA-Ogasawara; ISG=VERA-Ishigakijima; KYS=KVN-Yonsei; KUS=KVN-Ulsan; KTN=KVN-Tamna; TM65=TMRT65;

NS26=NSRT26; SH25=SHRT25; KM40=KMRT40; KSJ=Sejong22.

4.2.6 Baseline Length

The longest baseline length is related to astrometric accuracy as shown in Equations (9) and (10). Baseline lengths for EAVN astrometry are compiled in Table 22.

4.2.7 An accurate delay model for astrometry

The initial delay tracking model used by KJCC correlator is not sufficient for high precision position measurement (i.e., astrometry). Therefore, we provide a calibration table (called the delay re-calculation table) to PIs, where the difference between the correlator model and an accurate model is written in the calibration table. The accurate model can take into account the latest station coordinates, accurate source (i.e., target) coordinates, the most-updated Earth Rotation Parameters (EOPs), tropospheric and ionospheric delays (see [20] for details).

The calibration table can be loaded with the AIPS task TBIN. In order to receive the calibration table for astrometry data reduction, PI can contact EAVN help, eavnhelp(at mark)kasi.re.kr. The delivery of observation data and calibration table will take about three months after the observation.

4.2.8 Data Reduction

Generally, users are encouraged to carry out data reduction in consultation with contact person and/or support scientist in the KaVA/EAVN project group. Procedure of astrometric data reduction for VERA data has been summarized in previous papers (e.g. Fig. 11 in [11]; Fig. 5 in [10]). Basically, the procedure of data reduction for KaVA/EAVN data is consistent with that for VERA data, expect for few points.

For instance, parallactic angle should be corrected if the fast switching observation is conducted with single beam. The NRAO AIPS task "CLCOR" can be used for the calibration by setting the OPCODE = "PANG".

4.3 1-beam Hybrid (K/Q/W) Mode

KaVA will enable us to conduct VLBI observations in combinations of different types of antennas (antenna beams), receiving bands, recording rates (namely total band widths), and filtered base band channels in one observing session, whose cross correlation is still valid for the whole or some parts of KaVA. In such "hybrid" observing modes with KaVA, there are some modes that are available in the 2024A CfP described as follows.

Although VERA shall use only one of dual beams in a single frequency band (K or Q), the KVN is able to observe in two to three of K/Q/W bands simultaneously in a common observing session. Please check the KVN status report for W-band information:

https://radio.kasi.re.kr/status_report/status_report.php?site=kvn

Signal correlation for all the KaVA baselines is valid for the band in which both the KVN and VERA observe, while that for all the observed bands is valid for the KVN baselines.

Frequency allocations should be made separately to the KVN and VERA, including base band channels that are common between the two arrays in a specific band (K or Q). Note that the number of base band channels or the total bandwidth available per frequency band is limited, therefore brighter continuum sources should be selected for group-delay calibration.

4.4 Wide-field Imaging Mode

This mode is required to fully image 44 GHz methanol maser emissions associated with star-forming regions, which are generally distributed on the angular scale over 10 arcsec. The wide-field imaging (WFI) mode is achieved with an accumulation period shorter than the usual one of 1.6384 sec in Daejeon correlator at KJCC. Theoretically, the field of view (FoV) within an amplitude loss of 1%, 5%, and 10% is estimated on the basis of the time-average smearing effect due to a finite accumulation period [24]. The FoVs calculated for accumulation periods of 0.2048, 1.6384, and 3.2768 sec are summarized in Table 23, in the case of the highest angular resolution at Q-band of 0.6 mas with KaVA.

Table 23: FoV within a given amplitude loss in each accumulation period*.

	Aı	nplitude lo	OSS
	1.0%	5.0%	10.0%
Accumulation period	FoV	FoV	FoV
(sec)	(arcsec)	(arcsec)	(arcsec)
0.2048	8.6	19.4	27.4
1.6384	1.1	2.4	3.4
3.2768	0.5	1.2	1.7

^{*} Under an assumption of the highest angular resolution at Q-band of 0.6 mas with KaVA.

In the current available specification of Daejeon correlator, there is a trade-off between a shorter accumulation period and a larger number of IF channels to yield higher spectral resolution. The most highly recommended setup is the combination of C2 mode and an accumulation period of 0.2048 sec, in which both a sufficiently high velocity resolution (0.11 km s⁻¹ for 44 GHz methanol masers) and a sufficiently wide FoV (10 arcsec or more) can be obtained. Thus the recommended set-up for WFI mode is summarized in Table 24.

Table 24: Recommended set-up for WFI mode in the current situation.

Correlation	Sampling	Bandwidth	Accumulation	Spectral
mode	rate	$/\mathrm{IF}$	period	channels/IF
C2	1024 Mbps	128 MHz	$0.2048 \sec$	8,192

The evaluation for the WFI tests was done by the following two ways: comparing the data of an accumulation period of 0.1 sec produced in DiFX to those of 0.2048 sec in Daejeon correlator, and comparing the latter data to the same data but with averaging in 3.2768 sec. These ways provide us a chance to estimate whether such an isolated maser can be detected or not and how much rate of the amplitude loss occurs. The

evaluation might be updated on the basis of a comparison between a short-accumulation period data and a multi-tracking center data in the near future.

If you would like to require this WFI mode, please describe your requests in the following two items:

- Requested setting parameters for WFI in the proposal cover sheet
- Reasons for requiring WFI mode in the scientific justification

Finally, note that the file size of correlated data for WFI is as huge as ~600 GByte. We therefore recommend to check and improve the performance of your internet environment and personal computer as high as possible for comfortable data downloading and data processing, respectively. Please refer an example parameters in Table 25:

Table 25: Required performances of internet and personal computer.

Forward speed	$\geq 10 \text{ MByte s}^{-1}$
HDD/SSD volume	$\geq 1.5 \text{ TByte}$
RAM	$\geq 16 \text{ GByte}$

Here, the experiment to verify the time-average smearing effect due to a finite accumulation period has been done, however we will also verify the bandwidth smearing effect to KaVA observations in the near future.

4.5 Simultaneous K/Q Band Mode

Simultaneous K/Q-band data reception mode is available for KaVA, NRO45, and KSJ on a limited basis for open-use. Please note the following limitation: (1) K/Q simultaneous observations cannot be performed regularly but will be performed by setting up to two sessions in 2024A semester (where each slot spans approximately one—two week(s)) because VERA requires a special setup at the front-end for K/Q simultaneous reception. (2) The frequency setup is fixed as shown in Table 26. Especially when NRO45 joins, the frequency setup is strictly limited as in Table 26. The term of K/Q session will be determined depending on requests of approved proposals. (3) Frequency phase transfer (FPT) technique [23] is not applicable to the data obtained at NRO45. (4) 'Template method' for the amplitude calibration should be employed to the data obtained at NRO45 since the system noise temperature cannot be measured using the K/Q-band simultaneous reception system at Nobeyama. (5) Multi-frequency mode and dual-polarization mode cannot be employed simultaneously for the EAVN session in the 2024A semester.

A demonstrative observation and detailed performance of simultaneous K/Q-band observations with KaVA is presented in the Zhao et al. (2019). You can also check science cases with simultaneous multi-frequency VLBI observations [5].

4.6 Condition on the Usage of Nobeyama 45-m Telescope

In the 2024A semester, NRO 45-m telescope will not join the EAVN observations due to the problem in the hydrogen maser operated by the Mizusawa VLBI Observatory of NAOJ.

Table 26: Frequency setup for simultaneous K/Q band observation

Band	Frequency range	BBC channel	Polarization
Withou	t NRO45		
K-band	22.112 - 22.240 GHz	$32~\mathrm{MHz} \ge 4~\mathrm{channels}$	RCP
Q-band	42.812 - 42.940 GHz	$32~\mathrm{MHz}$ x 4 channels	\mathbf{LCP}
With N	RO45		
K-band	22.116 - 22.244 GHz	$16~\mathrm{MHz} \ge 8~\mathrm{channels}$	RCP
Q-band	42.816 - 42.944 GHz	$16~\mathrm{MHz} \times 8~\mathrm{channels}$	LCP

5 Observation and Data Reduction

5.1 Preparation of an EAVN Observation

You will be notified when your observation is scheduled by the EAVN scheduling officer. After the acceptance of proposals, users are requested to prepare the observing schedule file. Information about the user support is available at the EAVN web site:

https://radio.kasi.re.kr/eavn/user_support.php

Your schedule file must be submitted to eavnobs@kasi.re.kr one week before your observing date. If your schedule submission is delayed, your observation may not be assigned. For the EAVN schedule submission, PI should submit both a stand-alone vex file and a SCHED key file. In the vex file, please specify calibration procedures for hot/cold calibration, sky dipping, pointing, etc. We also request PIs to specify your correlation parameters at the beginning of the vex file (in case of EAVN observation) or in the key file (in case of KVN observation) for proper correlation processing. In particular, PIs who request for sub-array or dual-beam observations for EAVN should provide a frequency matching table for the correct correlation.

On your schedule, we strongly recommend to include at least two fringe finder scans, each lasting 5 or more minutes at the first and latter part of observation in order to search the delay and rate offsets for the correlation.

For EAVN which includes the large telescopes (TMRT65 and NRO45), regular pointing check is necessary at both K- and Q-bands. You should leave a 8-15 min gap every $\leq 1-2$ hr in your schedule file to allow this. Pointing check is done by the local operators. In addition, we strongly recommend to include frequent scans of a maser source and/or a bright compact continuum source located within 15° from the target. This allows a cross check of the amplitude calibration for TMRT65 and NRO45 along with the usual a priori method.

If you request the participation of the YAM32 and/or KMRT40 and/or NSRT26 antennas at C-band, it is mandatory to do gain calibration and absolute flux scaling by the template spectrum method. In this method, a strong and compact CH₃OH maser source that locates within 15° from the target source is observed with an interval of 1 hr or shorter. In particular during elevations lower than 20°, it is recommended to observe these calibrators every 30 min or shorter. Even if the YAM32 and/or KMRT40 and/or NSRT26 antennas are not included, it is recommended to observe the strong and compact CH₃OH maser source with the same interval as the cross-check for the gain curve and absolute flux scaling of the TMRT65 antenna as well. To select calibrators appropriated to your target sources, please see Section 3.10.

In the case of any observations for CH₃OH masers at 6.7 GHz in C-band, it is strongly recommended to request the C5 correlation mode (16 MHz \times 16 IFs) and the maximum spectral channels 8,192 for IF5 including the maser emission (corresponding to RF 6,664–6,680 MHz with the normal frequency set-up) to achieve the sufficient channel resolution of 1.953 kHz, yielding to the velocity resolution of \sim 0.088 km s⁻¹.

5.1.1 Sample Key Files for NRAO sched

From the 2023A semester, EAVN UST provides sample key files to be used for preparation of schedule files. Basic information and user guide are available on the EAVN website:

https://radio.kasi.re.kr/eavn/user support.php

There are collection of the inputs for the NRAO sched software. Files are available on the same EAVN website. For more details of NRAO sched, please refer to the NRAO website as listed in the above website. The above sample key files take into account special settings optimized to EAVN observations (e.g. fixed/nominal frequency setting recommended/required for each telescope). Thus, the EAVN users are strongly recommended to use the above sample key files. The detailed information will be updated on the EAVN website.

5.2 Observation and Correlation

EAVN members take full responsibility for observation and correlation process, and thus basically proposers will not be asked to take part in observations or correlations. Observations are proceeded by operators from each array and telescope, and correlated data is delivered to the users in approximately two months including the time for media shipping to KJCC at Daejeon.

After the correlation, the user will be notified where the data can be downloaded by e-mail. After one month later of a correlated data distribution to PIs, disk modules which contains raw observing data can be recycled without notice. Therefore, PIs should investigate the correlated output carefully. For re-correlation or raw data keeping of the data, PI should provide adequate evidence in order to justify his/her request. If there is an issue related to correlated data, PI should contact with the EAVN UST or the correlator team (kjcc (at-mark) kasi.re.kr), and not to ask KJCC members directly.

5.3 Data Reduction

For EAVN data reduction, the users are encouraged to reduce the data using the NRAO AIPS software package. The observation data and calibration data will be provided to the users in a format which AIPS can read.

As for the amplitude calibration, we will provide "ANTAB" files which include the system temperature information measured by the R-sky method and the information of the dependence of aperture efficiency on antenna elevation, except YAM32 and KMRT40 antennas where the gain calibration and absolute flux scaling have to be achieved via the template spectrum method in the AIPS task "ACFIT". A sample script for the template spectrum method is available on the EAVN website (see section 5.3.1). If the user needs weather information, the meteorological data of the temperature, pressure, and humidity during the observation can be provided.

5.3.1 Sample AIPS Recipes

EAVN UST will provide sample recipes for data calibration and imaging by using AIPS. These are simple script files for the following observation settings:

- KaVA observation of the 22 GHz H₂O maser
- EAVN observation of the 6.7 GHz CH₃OH maser
- EAVN phase-referencing observation at K-band
- RUN file for the KaVA phase-referencing astrometry of the 22 GHz H₂O maser

A sample script for the amplitude calibration procedure via the template spectrum method is available. Files are available the following EAVN web sites:

https://radio.kasi.re.kr/eavn/user_support.php

While these files cover only widely used basic setting but not all the available observation modes, they can be modified for your observation mode.

5.4 Policy of User Support

EAVN will not assign any support scientists to all the accepted proposals. If the proposers/observers have any inquiry about EAVN observations, they should contact with the EAVN UST and/or the relevant addresses as listed in Table 27. If the proposers need extensive support by the EAVN experts for schedule preparation and data analysis, they can request to assign a support scientist in the proposal cover sheet. UST will arrange the support scientist to the accepted proposals which request extensive support considering their science cases and its necessity.

5.5 Acknowledgment

All EAVN users (both proposers for using EAVN and data analysts using EAVN archive data) are asked to specify the following acknowledgment (or similar one) to EAVN in their publications.

This work is made use of the East Asian VLBI Network (EAVN), which is operated under cooperative agreement by National Astronomical Observatory of Japan (NAOJ), Korea Astronomy and Space Science Institute (KASI), Shanghai Astronomical Observatory (SHAO), Xinjiang Astronomical Observatory (XAO), Yunnan Astronomical Observatory (YNAO), National Astronomical Research Institute of Thailand (Public Organization) (NARIT), and National Geographic Information Institute (NGII), with the operational support by Ibaraki University (for the operation of Hitachi 32-m and Takahagi 32-m telescopes), Yamaguchi University (for the operation of VERA Iriki antenna).

Please include participating telescopes of your project in Acknowledgment of your publications.

5.6 Further Information

The users can contact any staff member of EAVN by e-mail (see Table 27).

Table 27: Contact addresses.						
Name	E-mail address*	Related Field				
Inquiry about proposal submission	eavnprop	Proposal-related requests/questions				
User support team	eavnhelp	User support in general, request for recalculation of correlator model				
Operation team	eavnobs	(phase-referencing) Observation-related requests/questions, schedule submission				

Correlation-related requests/questions,

correlated data distribution

References

Correlator team

[1] EAVN Status Report for the 2024A Semester: https://radio.kasi.re.kr/status report.php?cate=EAVN

kjcc

- [2] NRO web site: http://www.nro.nao.ac.jp/~nro45mrt/html/index-e.html
- [3] Cho, I. et al. 2017, PASJ, 69, 87
- [4] Cui, Y. Z. et al. 2021, RAA, 21, 205
- [5] Dodson, R. et al. 2017, ApJ, 834, 177
- [6] Hachisuka, K. et al. 2006, ApJ, 645, 337
- [7] Han, S.-T. et al. 2008, Int. J. Infrared Millimeter Waves, 29, 69
- [8] Han, S.-T. et al. 2013, PASP, 125, 539
- [9] Honma, M. et al. 2008, PASJ, 60, 951
- [10] Imai, H. et al. 2012, PASJ, 64, 142
- [11] Kurayama, T. et al. 2011, PASJ, 63, 513
- [12] Lee, S.-S. et al. 2015, JKAS, 48, 229
- [13] Martí-Vidal, I. et al. 2010, A&A, 515, 53
- [14] Nagayama, T. et al. 2015, PASJ, 67, 65
- [15] Oh, S.-J. et al. 2011, PASJ, 63, 1229
- [16] Okada, T. et al. 2020, PASJ, 71, 7
- [17] Ott, M. et al. 1994, A&A, 284, 331

^{*:} Add @kasi.re.kr to the address.

- [18] Oyama, T. et al. 2016, PASJ, 68, 105
- [19] Reid, M. J. & Honma, M. 2014, ARA&A, 52, 339
- [20] Sakai, N. et al. 2023, PASJ, 75, 208
- [21] Yonekura, Y. et al. 2016, PASJ, 68, 74
- [22] Yoo, S. M. et al. 2018, JKAS, 51, 143
- [23] Zhao, G. Y., et al. 2019, JKAS, 52, 23
- [24] Proceedings from the 1988 synthesis imaging workshop in NRAO, Chapter 13 in Synthesis Imaging in Radio Astronomy: A Collection of Lectures from the Third NRAO Synthesis Imaging Summer School:
 - http://www.aspbooks.org/a/volumes/table_of_contents/?book_id=118